Seasonal sea surface temperature anomaly prediction for coastal ecosystems

CrossMark

Charles A. Stock [a,*], Kathy Pegion [b], Gabriel A. Vecchi [a], Michael A. Alexander [c], Desiree Tommasi [a], Nicholas A. Bond [d], Paula S. Fratantoni [e], Richard G. Gudgel [a], Trond Kristiansen [f], Todd D. O'Brien [g], Yan Xue [h], Xiasong Yang [a,i]

[a] NOAA Geophysical Fluid Dynamics Laboratory, Princeton University Forrestal Campus, 201 Forrestal Road, Princeton, NJ 08540-6649, USA
[b] George Mason University, Dept of Atmospheric, Oceanic and Earth Sciences, 4400 University Drive, MS6C5, Fairfax, VA 22030, USA
[c] NOAA Earth System Research Laboratory, Physical Sciences Division, 325 Broadway R/PSD1, Boulder, CO 80305-3328, USA
[d] University of Washington, Joint Inst. for the Study of the Atmos. and Ocean, Room 2074, Bldg3, NOAA Sandpoint, 7600 Sand Point Way NE, Seattle, WA 98115, USA
[e] NOAA/NMFS Northeast Fisheries Science Center, Woods Hole, MA 02543, USA
[f] Institute of Marine Research, Bergen, Norway
[g] NOAA/NMFS-ST Marine Ecosystems Division – F/ST7, SSMC-III – Rm 12535, 1315 East-West Hwy, Silver Spring, MD 20910, USA
[h] NOAA/CPC National Centers for Environmental Prediction, Room 3005, NCWCP, 5830 University Research Court, College Park, MD 20740, USA
[i] University Corporation for Atmospheric Research, Boulder, CO 80305, USA

ARTICLE INFO

ABSTRACT

Sea surface temperature (SST) anomalies are often both leading indicators and important drivers of marine resource fluctuations. Assessment of the skill of SST anomaly forecasts within coastal ecosystems accounting for the majority of global fish yields, however, has been minimal. This reflects coarse global forecast system resolution and past emphasis on the predictability of ocean basin-scale SST variations. This paper assesses monthly to inter-annual SST anomaly predictions in coastal "Large Marine Ecosystems" (LMEs). We begin with an analysis of 7 well-observed LMEs adjacent to the United States and then examine how mechanisms responsible for prediction skill in these systems are reflected in predictions for LMEs globally. Historical SST anomaly estimates from the 1/4° daily Optimal Interpolation Sea Surface Temperature reanalysis (OISST.v2) were first found to be highly consistent with *in-situ* measurements for 6 of the 7 U.S. LMEs. Thirty years of retrospective forecasts from climate forecast systems developed at NOAA's Geophysical Fluid Dynamics Laboratory (CM2.5-FLOR) and the National Center for Environmental Prediction (CFSv2) were then assessed against OISST.v2. Forecast skill varied widely by LME, initialization month, and lead but there were many cases of high skill that also exceeded that of a persistence forecast, some at leads greater than 6 months. Mechanisms underlying skill above persistence included accurate simulation of (a) seasonal transitions between less predictable locally generated and more predictable basin-scale SST variability; (b) seasonal transitions between different basin-scale influences; (c) propagation of SST anomalies across seasons through sea ice; and (d) re-emergence of previous anomalies upon the breakdown of summer stratification. Globally, significant skill above persistence across many tropical systems arises via mechanisms (a) and (b). Combinations of all four mechanisms contribute to less prevalent but nonetheless significant skill in extratropical systems. While continued refinement of global climate forecast systems and observations are needed to improve coastal SST anomaly prediction and extend predictions to other ecosystem relevant variables (e.g., salinity), present skill warrants close examination of forecasts for marine resource applications.

Published by Elsevier Ltd.

1. Introduction

Marine ecosystems are strongly affected by seasonal to decadal-scale climate variations (e.g., Lehodey et al., 2006). Sea surface temperature (SST) anomalies are often both leading

indicators and important drivers of these ecosystem fluctuations (Drinkwater et al., 2010; Mueter et al., 2009; Ottersen et al., 2010). Indeed, ecosystem states are often characterized as "warm" or "cold", with the understanding that this carries implications for diverse ecosystem characteristics including fish and zooplankton distributions (e.g., Beaugrand, 2003; Mackas et al., 2007; Nye et al., 2009; Pinsky et al., 2013), fish recruitment (e.g., Hunt et al., 2011; Kristiansen et al., 2011; Mantua et al., 1997; Planque

and Fredou, 1999), and phytoplankton bloom and sea ice phenology (e.g., Stabeno et al., 2001). Skillful prediction of ocean temperature anomalies thus has considerable potential for use in dynamic marine resource management (Hobday et al., 2014).

The development of dynamical global climate forecast systems over the past two decades (e.g., Goddard et al., 2001; Kirtman et al., 2014) has helped realize this potential. Pioneering applications of sea surface temperature (SST) anomaly predictions have been developed for coral bleaching on the Great Barrier Reef (Spillman and Alves, 2009; Spillman et al., 2011, 2013), avoidance of southern Bluefin Tuna bycatch in eastern Australia (Hobday et al., 2011) and salmon farm management in Tasmania (Spillman and Hobday, 2014). Critical assessment of SST anomaly prediction skill in global climate forecast systems, however, has been strongly skewed toward basin-scale modes of SST variation, particularly the El Nino-Southern Oscillation (ENSO, e.g., Barnston et al., 2012 and references therein; Jin et al., 2008). This emphasis reflects the strong theoretical basis for ENSO predictability (Battisti and Hirst, 1989; Bjerknes, 1969; Schopf and Suarez, 1988; Wyrtki, 1975; Zebiak and Cane, 1987), the relative success of ENSO prediction, and the large impact of ENSO on regional surface air temperature and precipitation patterns that have long been a focal point of seasonal prediction efforts (Barnett and Preisendorfer, 1987; Livezey and Smith, 1999; Livezey and Timofeyeva, 2008; Peng et al., 2012; Quan et al., 2006; Ropelewski and Halpert, 1986, 1987). Predicting SST anomalies is thus often viewed as a first step toward "user relevant seasonal climate anomalies" (Stockdale et al., 2011).

For marine resources, SST anomalies are of direct interest. Globally, the total economic value of marine fisheries and associated industries has been estimated at 225–240 billion dollars year^{-1} based on 2003 data (Dyck and Sumaila, 2010). Nearly half of the global marine fish landings contributing to this value were caught within 100 km of shore in waters less than 100 m deep (Nellemann et al., 2008). These shelf regions account for only 7.5% of ocean area, but their disproportionate contribution to global fish yields provides great impetus for skillful shelf-scale SST anomaly prediction. Several factors, however, make this difficult. First, global SST reanalyses often used as "observations" in forecast assessments can be challenged by sharp hydrographic gradients and complex water properties in coastal systems (e.g., Barton and Casey, 2005; Chelton and Wentz, 2005; Hughes et al., 2009; Smit et al., 2013). Second, the coarse resolution of global forecast systems (~0.5–2° ocean and atmosphere resolution) degrades the representation of shelf-scale dynamics (Stock et al., 2011). Third, prominent sources of local variation disconnected from predictable large-scale patterns may degrade forecast skill (e.g., Spillman and Alves, 2009).

The objectives of this contribution are to (1) assess seasonal SST anomaly predictions from two state-of-the-art global climate forecast systems across globally distributed coastal marine ecosystems, and (2) elucidate the mechanisms underlying cases with high forecast skill; particularly where skill significantly exceeds that of persistence forecasts. Our analysis begins with a detailed examination of SST anomaly prediction for 7 well-observed Large Marine Ecosystems (LMEs) covering United States coastal waters (Fig. 1). A progressive approach is used to identify forecast bottlenecks within these systems, starting with an assessment of the consistency of 1/4° daily Optimal Interpolation Sea Surface Temperature reanalysis (OISST.v2, Reynolds et al., 2007) against unprocessed in-situ observations, and ending with an assessment of mechanisms underlying skill above persistence. We then extend analysis across LMEs globally to identify additional systems where achieved skill offers a high potential for marine resource applications. We conclude with a discussion of the strengths and limitations of seasonal coastal ocean forecasts, including prospects for improvement.

2. Methods

2.1. Large Marine Ecosystems (LMEs)

LMEs are defined as "coherent ocean areas generally along continental margins whose ecological systems are characterized by similarities in bathymetry, hydrography, and biological productivity, and whose plant and animal populations are inextricably linked to one and other in the food chain" (Sherman and Alexander, 1986). While the details of any given LME relative to this definition can be debated, LMEs have been adopted as units to implement ecosystem-based marine resource management. Descriptions of all 66 Large Marine Ecosystems can be found at www.edc.uri.edu and a map is also included in the Supporting material.

We begin our analysis with a detailed analysis of the 7 LME's shown in Fig. 1: The East Bering Sea (EBS), the Gulf of Alaska (GoA), the California Current (CC), the Insular Pacific–Hawaiian Island (IP–H), the Gulf of Mexico (GoM), the Southeast United States (SEUS) continental shelf, and the Northeast United States (NEUS) continental shelf. These LMEs benefit from relatively dense observational networks to build confidence in retrospective anomaly estimates. Furthermore, retrospective anomaly estimates (Reynolds et al., 2007, see Section 2.3) suggest that spatially resolved SST anomalies at 1/4° resolution are generally coherent with the LME-average anomaly (mean correlations ~0.7, Table 1). The 7 LMEs offer significant contrasts in area, SST variability, bathymetry, local dynamics, and adjacent basin-scale processes (Table 1). As will be shown in Section 3, they also offer significant contrasts in the success of seasonal SST anomaly forecasts. Following this, we explore predictions across LMEs globally, highlighting where mechanisms similar to those responsible for skill above persistence within the 7 U.S. LMEs contribute to successful forecasts in other systems.

2.2. Global climate forecast systems

We considered two dynamical seasonal forecast systems: The NOAA Geophysical Fluid Dynamics Laboratory's CM2.5-FLOR prediction system (Vecchi et al., 2014) and the National Centers for Environmental Prediction Climate Forecast System version 2 (Saha et al., 2014). The characteristics of these systems are summarized in Table 2. Each system consists of coupled ocean, atmosphere, and land dynamics components combined with different approaches for forecast initialization and ensemble forecasting. CM2.5-FLOR is distinguished by its higher atmospheric resolution (~50 km) and the availability of 12 month forecasts, while CFSv2 features higher ocean resolution (~50 km over most regions) and provides 9 month forecasts.

CM2.5-FLOR retrospective forecasts are from the "B01" configuration and use 12 ensemble members initialized on the first of each month between 1982 and 2009 based on GFDL's Ensemble Coupled Data Assimilation system (ECDA, Zhang et al., 2007). Forecasts were obtained from the GFDL archive, but are also available from GFDL's data portal (data1.gfdl.noaa.gov) and, after regridding, in the North American Multi-Model Ensemble (NMME) database (Kirtman et al., 2014). Maintaining the native model grid proved useful for analyzing mechanisms underlying skill above persistence (see Section 2.5). CFSv2 forecast data was obtained for the same time period from the NMME database. For CFSv2, four forecasts, each with a 9-month integration, were made every 5 days with initializations based on CFSv2 assimilation system (Saha et al., 2010; Xue et al., 2011). We limited our CFSv2 calculations to the 16 ensemble members, started within 15–20 days of the first lead month. That is, forecasts assessed for the 9 month
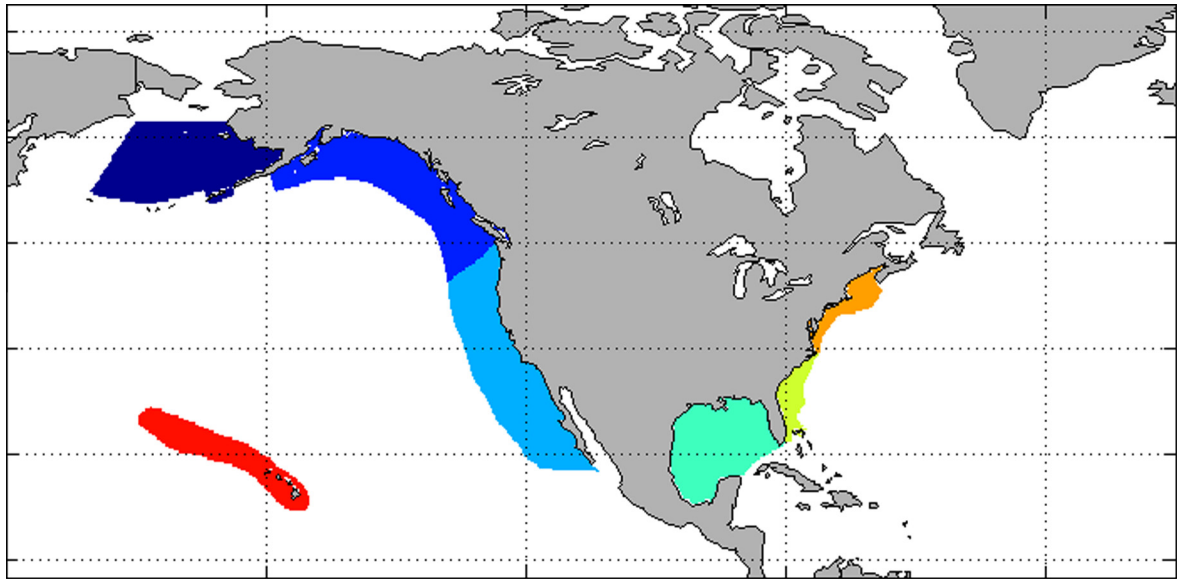
Fig. 1. Seven Large Marine Ecosystems subjected to detailed analysis in this study: the eastern Bering Sea (EBS, dark blue); the Gulf of Alaska (GoA, medium blue); the California Current (CC, light blue); Insular Pacific Islands–Hawaii (IP–H, dark red); the Gulf of Mexico (GoM, blue–green); Southeast United States (SEUS, green); and the Northeast U.S. (NEUS, orange).

Table 1

Summary of the characteristics of the LMEs subjected to detailed forecast analysis herein. Area is in $km^2/10^5$. ACC here is the mean correlation of monthly OISST.v2 anomalies from each $1/4°$ grid cell with the average anomaly for the LME and provides a measure of the coherence of SST anomalies across the LME. Anomalies were standardized by the standard deviations of anomalies for each grid cell prior to the calculation. The standard deviation of LME-average monthly anomalies from NOAA OISST.v2 is given by σ_{LME}.

LME	Area ($/10^5$)	Mean ACC	σ_{LME}	Notable properties
East Bering Sea (EBS)	11.9	0.71	0.56	Partially enclosed basin; broad shallow shelf; sea-ice present during some seasons
Gulf of Alaska (GoA)	14.2	0.80	0.59	Includes narrow shelf and deeper off-shore waters; broad exposure to ocean basin; at downstream terminus of North Pacific current
California Current (CC)	22.0	0.72	0.56	Includes narrow shelf and deeper offshore waters; broad exposure to ocean basin; eastern boundary upwelling system
Gulf of Mexico (GoM)	15.2	0.70	0.44	Partially enclosed basin with mix of shallow shelf and deep off-shore waters
Southeast U.S. (SEUS) shelf	3.0	0.72	0.49	Relatively small, narrow shelf adjacent to western boundary current
Northeast U.S. (NEUS) shelf	3.1	0.73	0.65	Relatively small, shallow shelf system near western boundary current
Insular Pacific–Hawaiian (IP–H)	9.8	0.66	0.41	Oceanic system

January–September window are based on forecast ensemble members initialized during the latter half of December rather than on January 1st as in CM2.5-FLOR. We note that this puts CFSv2 at a slight lead-time disadvantage when comparing skill relative to CM2.5-FLOR.

2.3. Historical SST anomaly estimates

NOAA version 2 optimally interpolated daily high-resolution-blended sea surface temperature estimates (OISST.v2, Reynolds et al., 2007) were used to provide spatially and temporally continuous SST anomaly estimates with which to evaluate retrospective forecasts. The version used herein covers 1981–present and is constructed via optimal interpolation of SST measurements from infrared (AVHRR) satellite sensors and in-situ bucket, buoy and ship-based observations from the ICOADS database (Worley et al., 2005) to a spatial resolution of $1/4°$ and a temporal resolution of 1 day. The e-folding scale for the weighting observation in the OI scheme ranges from 100 to 250 km.

The ability of OISST.v2 ocean state estimates to resolve the direction and magnitude of hydrographic anomalies within highly dynamic coastal systems has not been extensively tested. Where evaluations of OISST.v2 or other products have been made, results were mixed (Barton and Casey, 2005; Chelton and Wentz, 2005; Hughes et al., 2009; Smit et al., 2013). OISST.v2 was thus evaluated

against unprocessed, *in-situ* observations at the LME-scale prior to use in forecast evaluation.

In-situ SST measurements for the LME's in Fig. 1 were extracted from the 2013 NOAA World Ocean Database (WOD13, Boyer et al., 2013) for the period 1982–2010, the same period for which retrospective forecasts were made. OISST.v2 estimates were sampled at the location and time of each *in-situ* observation. A common 1982–2010 reference climatology was then subtracted from both the WOD13 observations and the OISST.v2 estimates, yielding paired point anomaly estimates. Since coastal LME's have strong spatial and temporal SST gradients, the high-resolution OISST.v2 climatology was used as the reference, noting that any deficiencies in the OISST.v2 climatology will be reflected in biases between WOD13 and OISST.v2-based anomalies. WOD13 and OISST.v2 anomalies for each LME were binned and the mean taken at annual, seasonal and monthly intervals. Correlation, bias, and standard deviations were then calculated to assess the consistency in the sign and magnitude of WOD13 and OISST.v2 anomalies.

OISST.v2 anomalies are also compared with GFDL-ECDA and NCEP-CFSv2 assimilations used to initialize the forecasts. OISST.v2 is used within both the GFDL-ECDA and NCEP-CFSv2 data assimilation schemes (Table 2, Xue et al., 2011; Zhang et al., 2007). Within CFSv2, OISST.v2 is treated separately from the 3DVAR scheme used to for other data types. Surface ocean temperatures

Table 2
Summary of forecast system characteristics with relevant references for more details.

Forecast system	GFDL CM2.5-FLOR B01 (Vecchi et al., 2014)	NCEP CFSv2 (Saha et al., 2014)
Atmospheric/land model	50 km × 50 km Atmosphere from GFDL's CM2.5 climate model, LM3 land model (Delworth et al., 2012)	T126 (~100 km horizontal resolution), 64 sigma-pressure coordinates in vertical; NOAH land surface model (Ek et al., 2003)
Ocean/sea ice model	1° MOM4p1 ocean telescoping to 1/3° meridional spacing near the equator from GFDL's CM2.1 climate model (Delworth et al., 2006; Griffies et al., 2005)	MOM4p0, 1/2° resolution, telescoping to 1/10° meridional spacing near the equator (Griffies et al., 2004; Saha et al., 2010)
Forecast initialization	Ocean and ice conditions from GFDL's Ensemble Coupled Data Assimilation system (Zhang et al., 2007); atmosphere initialized from suite of SST forced atmosphere-land-only simulations	NCEP's Climate Forecast System Reanalysis (Saha et al., 2010; Xue et al., 2011)
Forecast ensemble properties	12 Month forecasts of 12 member ensembles started the first of each month	9 Month forecasts with 4 ensemble members starting every 5th day. Used 16 ensemble members within 15–20 days of the first of the month for analyses herein

are strongly relaxed toward OISST.v2, making good agreement inevitable. In GFDL-ECDA, however, OISST.v2 is treated as other data types within the Ensemble Kalman Filter approach. The need to reconcile the model with OISST.v2 at coastal scales within the ECDA assimilation does not guarantee a good fit, making this comparison a meaningful initial step in the forecast evaluation.

2.4. Assessment of SST anomaly forecasts

Prediction skill of the LME average SST anomaly was assessed using the anomaly correlation coefficient (ACC) between the forecast (F') and observed (O') anomalies as a function of initialization month (m) and lead time (t):

$$\text{ACC}(t,m) = \frac{\sum_{\alpha=1}^{N}(F'_\alpha(t,m) \times O'_\alpha(t,m))}{\sqrt{\sum_{\alpha=1}^{N}F'_\alpha(t,m)^2 \sum_{\alpha=1}^{N}O'_\alpha(t,m)^2}} \quad (1)$$

Monthly forecast and observed anomalies are not de-trended or filtered. The sample for calculating the ACC at each lead and start month is drawn from the ensemble mean trajectories of 28 forecasts initiated for a given start month between 1982 and 2009 ($N = 28$ in Eq. (1)). To correct for drift in the forecast system, forecast anomalies are calculated relative the lead-dependent climatology formed from the same 28 ensemble mean forecasts for each initialization month. The ACC ranges from −1 to 1 and quantifies the extent to which SST variability in the forecast and the observations coincide. A common reference of a minimum usable forecast skill is an anomaly correlation ⩾0.5 (Roads, 1986). A weakness of the ACC is that it does not detect systematic differences in anomaly variance between the forecast and the observations. We provide estimates of the root mean squared deviance (RMSD) in the Supporting material (Figs. S18–S34), while noting that rescaling SST anomalies provides a means of adjusting for magnitude biases when SST anomalies are of direct interest (e.g., see discussion in Stockdale et al., 2011).

ACC values were calculated for both dynamical forecast systems (i.e., CM2.5 FLOR and CFSv2) and a "persistence forecast" that presumes the prior month's OISST.v2 anomaly persists across all leads (von Storch and Zweirs, 1999). Skill relative to persistence is a key measure of the added value of dynamical forecast systems (see Sections 3.3 and 4).

ACC significance was assessed after correcting degrees of freedom for autocorrelation using the methodology described in Bretherton et al. (1999):

$$N_{eff} = \frac{N}{\sum_{t=0}^{t=N-1}\left(1 - \frac{t}{N}\right)r_t^F r_t^O} \quad (2)$$

where $N = 28$ is the number of samples in the forecast (F) and observed (O) time series, and r_t^F and r_t^O are estimates of the

autocorrelation in each time series at lag t. Tests were carried out to determine if (a) the dynamical forecast ACC is significantly greater than 0; and (b) the dynamical forecast ACC is significantly greater than the persistence forecast ACC. Both use a Fisher's z transformation (Fisher, 1915, 1924; von Storch and Zweirs, 1999), where sample estimates of the correlation coefficient are transformed with:

$$Z_{F,O} = 0.5\ln[(1 + r_{F,O})/(1 - r_{F,O})] \quad (3)$$

where $r_{F,O}$ is the correlation between the forecast and observed time series. The quantity $Z_{F,O}$ then follows a z distribution with $N_{eff} - 3$ degrees of freedom. To test (a), a one-sided 90% confidence interval was calculated for Z, transformed back to correlation space using the Fisher's z transformation, and compared against $r = 0$. To assess (b), 1000 realizations were drawn from the respective z distributions of the persistence and dynamical forecasts. Enhancement of skill was deemed 90% significant for those cases in which the dynamical forecast correlation was greater than the persistence forecast 90% of the time.

2.5. Understanding skill above persistence

Select forecasts exhibiting an ACC > 0.5 and significant skill above persistence are singled out for more detailed analysis. The evolution of SST anomalies between forecast initialization and the forecast window is determined through a combination of horizontal and vertical ocean transport and net atmosphere–ocean heat flux variations (e.g., Deser et al., 2010). We diagnose the roles of these processes using spatial correlation analysis to identify prominent contributors to skill above persistence. Finer parsing of system-specific heat budgets (e.g., Benthuysen et al., 2014; Frankignoul, 1985) would require additional diagnostics and is beyond the scope of this contribution.

The role of horizontal transport is examined through the correlation between the observed LME mean SST anomaly during a forecast window and spatially explicit SST anomalies within the forecast initialization and/or earlier in the forecast. Forecast surface currents are enlisted to elucidate transport pathways.

The role of vertical transport is assessed through the correlation between the observed LME mean SST anomaly during a forecast window and ocean temperature anomalies at depth during the forecast initialization and/or earlier in the forecast. The maximum mixed layer depth during the period between the initialization and forecast window is used to identify depth strata that influence forecast SST anomalies.

The role of the atmosphere–ocean heat fluxes in shaping forecast anomalies is assessed through the correlation between the LME mean SST anomaly during the forecast window and the forecast net atmosphere–ocean heat flux anomalies during months prior to the forecast window.

In all cases, the significance of correlations was tested with the methodology described in Section 2.4. Only correlations whose magnitude is significantly different than zero at the 90% confidence level are shown.

3. Results

3.1. Evaluation of historical SST anomaly estimates

OISST.v2 anomalies were found to be consistent in magnitude and direction with raw WOD13 anomalies at the LME-scale for six of the seven LMEs in Fig. 1 (Table 3). Correlation in the six consistent systems was highest at annual scales (>0.9), but remained >0.75 for monthly anomalies. The exception was the Southeast United States (SEUS), where OISST.v2 and WOD13 anomalies were less correlated ($r = 0.48–0.60$). The SEUS LME is the smallest of those considered (Table 1) and is immediately adjacent to the Gulf Stream, creating a sharp hydrographic contrast that may contribute to the WOD13 and OISST-v2 inconsistencies.

OISST.v2 is also biased warm relative to WOD13 measurements in most systems (Table 1). The bias is generally ∼5–10% of the scope of the anomalies (i.e., the 4 standard deviation width), but is somewhat larger (∼20%) for the Insular Pacific/Hawaii (IP/H) LME. It could reflect differences in the representative depth of satellite versus in-situ SST measurements (e.g., May et al., 1998). We note, however, that bias does not affect the ACC metric central to this study.

The forecast initial conditions for the GFDL and NCEP forecasts generally agree with each other and the OISST.v2 anomalies (Table 4). As noted in Section 2, this agreement is not surprising for CFSv2 due to tight relaxation toward OISST.v2 at the ocean surface. For GFDL-ECDA, it confirms that the forecast initialization still contains anomalies consistent with OISST.v2 after reconciliation of coarse global model dynamics and OISST.v2 in the relatively small, dynamic coastal systems of interest herein. The only LMEs showing signs of degraded agreement with OISST.v2 in ECDA are the NEUS and SEUS systems; small LMEs influenced by western boundary currents not well resolved in 1° ocean models (e.g., Delworth et al., 2012).

In combination, Tables 3 and 4 suggest that accurate retrospective SST estimates at the LME-scale and accurate SST initialization are not primary limiters of forecast skill assessment for 6 of the 7 LMEs in Fig. 1. We thus proceed with the forecast skill assessment

Table 3

Comparison of anomalies on annual, seasonal and monthly time scales from the High-Resolution SST reanalysis OISST.v2 with World Ocean Database anomalies for each LME. Comparisons are based on 1982–2010 to match the hindcast data. Bias is the mean difference between WOD13 data points and the OISST.v2 climatology, with negative values indicating warm bias in OISST.v2. Biases are normalized by the four standard deviation width of the anomalies between WOD13 data and the OISST.v2 climatology (σ_w) to indicate the size of the bias relative to the spread of the anomalies. The ratio of standard deviations of the OISST.v2 (σ_{OI}) and WOD13 anomalies assesses damping (<1) or amplification (>1) in OISST.v2 relative to WOD13.

	EBS	GoA	CC	IP–H	GoM	SEUS	NEUS
Annual							
r	0.91	0.94	0.96	0.90	0.93	0.52	0.93
Bias/$4\sigma_w$	−0.12	−0.09	−0.07	−0.25	−0.07	−0.10	0.06
σ_{OI}/σ_w	0.94	1.09	0.96	1.23	0.96	1.08	0.82
Season							
r	0.91	0.88	0.93	0.89	0.84	0.60	0.87
Bias/$4\sigma_w$	−0.08	−0.10	−0.07	−0.21	−0.03	−0.08	0.04
σ_{OI}/σ_w	0.92	1.05	0.96	1.16	0.88	0.93	0.85
Month							
r	0.75	0.85	0.92	0.86	0.82	0.48	0.83
Bias/$4\sigma_w$	−0.06	−0.09	−0.07	−0.17	−0.02	−0.06	0.03
σ_{OI}/σ_w	0.88	1.03	0.96	1.12	0.89	0.82	0.90

Table 4

Comparison of OISST.v2 anomalies against reanalyses used to initialize CM2.5-FLOR and CFSv2 forecasts. Comparisons are based on initiations from 1982 through 2009 (i.e., for forecasts stretching from 1982 to 2010) and averages across all grid cells within an LME (in contrast to the point-wise comparisons against WOD13 data in Table 3). Biases are reported as the mean differences between the forecast reanalysis and OISST.v2 such that positive values indicate a warm bias in the forecast initialization. Note that CFSR is strongly relaxed to OISST.v2 and that there are discrepancies between OISST.v2 and WOD13 data in the SEUS (Table 3).

	EBS	GoA	CC	IP–H	GoM	SEUS	NEUS
GFDL-ECDA							
r	0.89	0.95	0.94	0.89	0.81	0.58	0.70
Bias/$4\sigma_{OI}$	0.00	0.00	0.00	0.00	0.00	0.00	0.00
$\sigma_{ECDA}/\sigma_{OI}$	1.00	1.07	1.01	0.89	1.07	1.19	1.39
NCEP-CFSR							
r	0.99	1.00	1.00	1.00	0.99	0.98	0.94
Bias	0.00	0.00	0.00	0.00	0.00	0.00	0.00
$\sigma_{CFSR}/\sigma_{OI}$	1.02	1.01	0.99	1.02	0.98	1.03	1.01

and diagnosis, while noting that many other ecosystem relevant variables may not meet these criteria (e.g., see sea surface salinity discussion in Section 4).

3.2. SST anomaly forecast skill and underlying mechanisms across U.S. LMEs

Forecast skill (ACC) for the dynamical forecast systems (GFDL CM2.5-FLOR, NCEP CFSv2) and persistence forecasts are summarized for the 7 U.S. LMEs in Figs. 2 and 3. Forecast skill varies widely by LME, initialization month (x-axis of figure panels), and forecast lead (y-axis of figure panels). There are many cases, however, of high ACCs that significantly exceed persistence forecast skill. Many of these occur with leads of 6 months or more. *Global climate forecast systems thus have notable coastal SST anomaly forecasting skill for many systems, at least at the LME-scale, despite relatively coarse oceanic and atmospheric resolution.*

Differences in prediction skill between the two forecast systems are generally secondary to cross-LME predictability contrasts. We thus focus analysis on the latter, particularly understanding mechanisms generating skill above persistence.

East Bering Sea (EBS) forecasts (Fig. 2, top row) are characterized by elevated ACCs for April 1 to October 1 initializations predicting into the early winter (i.e., in the CM2.5 FLOR forecast, note the right triangle of red/orange colors extending upward from initialization month 4, April 1, out 9 months on the y-axis, and then descending steadily until elevated ACCs for month 10, October 1, initializations are apparent out to 3 month or less). The diagonal forming the upper bound of this right triangle corresponds to a December anomaly forecast. Hence, from April to October, one can forecast SST anomalies out to December with some skill. The paucity of white triangles for forecasts within this region of elevated skill, however, indicate that dynamical model forecast ACCs do not generally exceed the skill of the persistence forecast (Fig. 2, top row, right panel) by a significant margin.

ACCs sharply decline and become statistically insignificant as April to October initialized EBS forecasts are extended through the winter to the early spring (note the white/orange limb with a width of 3–5 months extending diagonally downward above the right triangle of high skill discussed above). Surprisingly, forecast skill in the EBS can be reestablished after winter (e.g., note the August 1 initialized forecast for the following May–July in CM2.5 FLOR). This occurs in both dynamical forecast systems and, to a lesser degree, in the persistence forecast. It can be understood through the inverse relationship between forecast EBS sea ice mass anomalies during the seasonal sea ice peak (March) and SST anomalies the following summer (Fig. 4). Sea-ice serves as
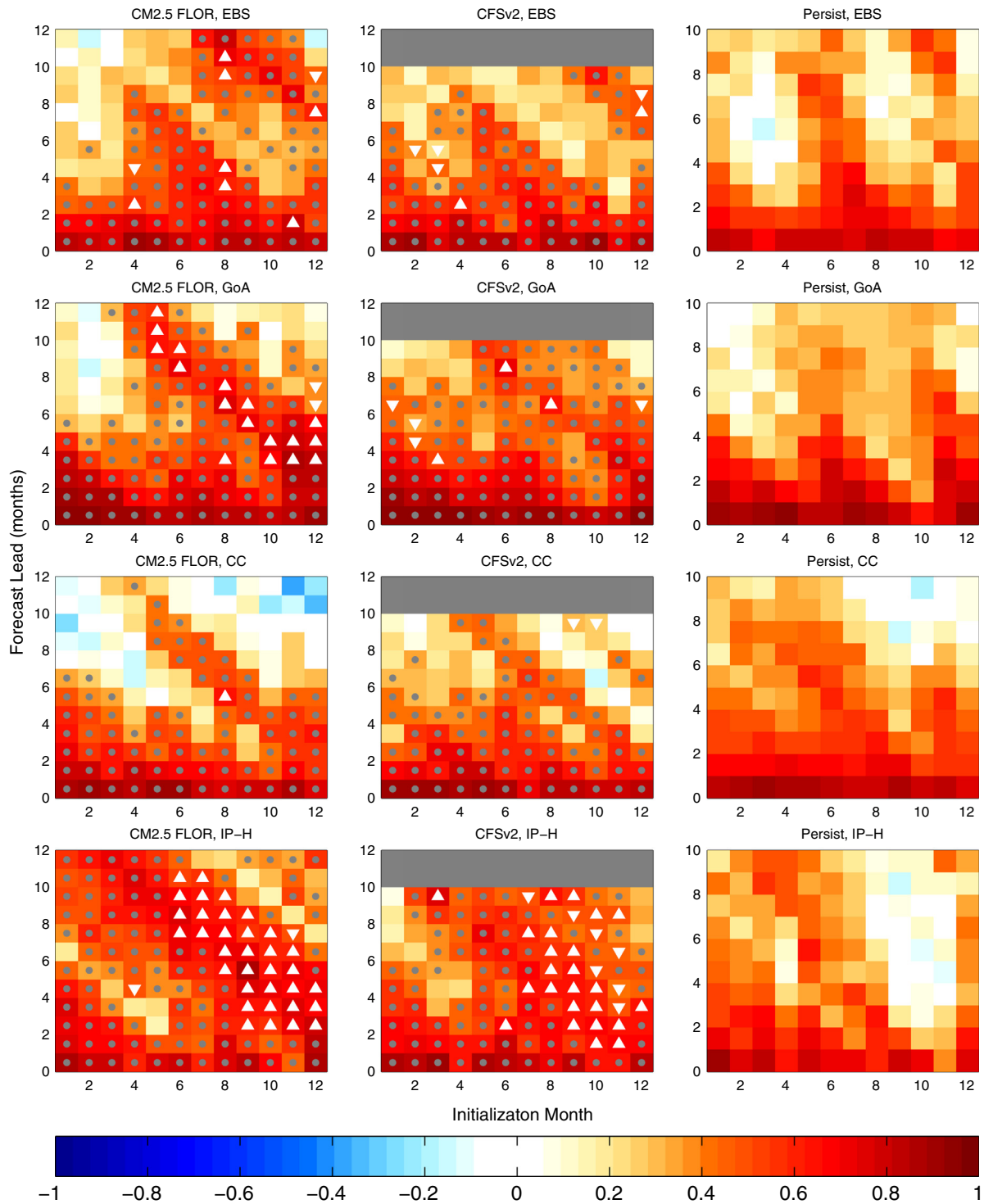
Fig. 2. Anomaly correlation coefficients (ACCs) as a function of forecast initialization month (x-axis) and lead time (y-axis). Initialization month 1 corresponds to January 1 initialization in CM2.5 FLOR and initialization during the latter half of December in CFSv2 (see Section 2.2). The lower left box (x = 1, y = 0–1) thus corresponds to a January forecast and the lower right a December forecast. Gray dots indicate ACCs significantly above 0 at 5% level; white upward triangles indicate ACCs significantly above persistence at the 10% level with ACC > 0.5; downward triangles indicate ACCs above persistence at 10% level with ACC < 0.5.

reservoir for carrying fall SST anomalies across the winter season to the following spring in the EBS – with high sea ice mass carrying cold SST signals and low sea ice mass carrying warm. This mirrors mechanisms invoked to explain sea-ice predictability in the Arctic whereby melt patterns during previous years leave SST imprints that impact ice extent during the following ice growth season (Blanchard-Wrigglesworth et al., 2011).

The sea-ice mechanism illustrated in Fig. 4 further suggests that winter/early spring initialized prediction may generate ACCs above persistence with accurate initialization of sea-ice mass. Such predictions, however, have little skill in CM2.5 FLOR. They are somewhat better CFSv2, but improved sea-ice initialization may still offer a means of improving spring/summer SST anomaly forecast skill in the EBS for both forecast systems (see Section 4).
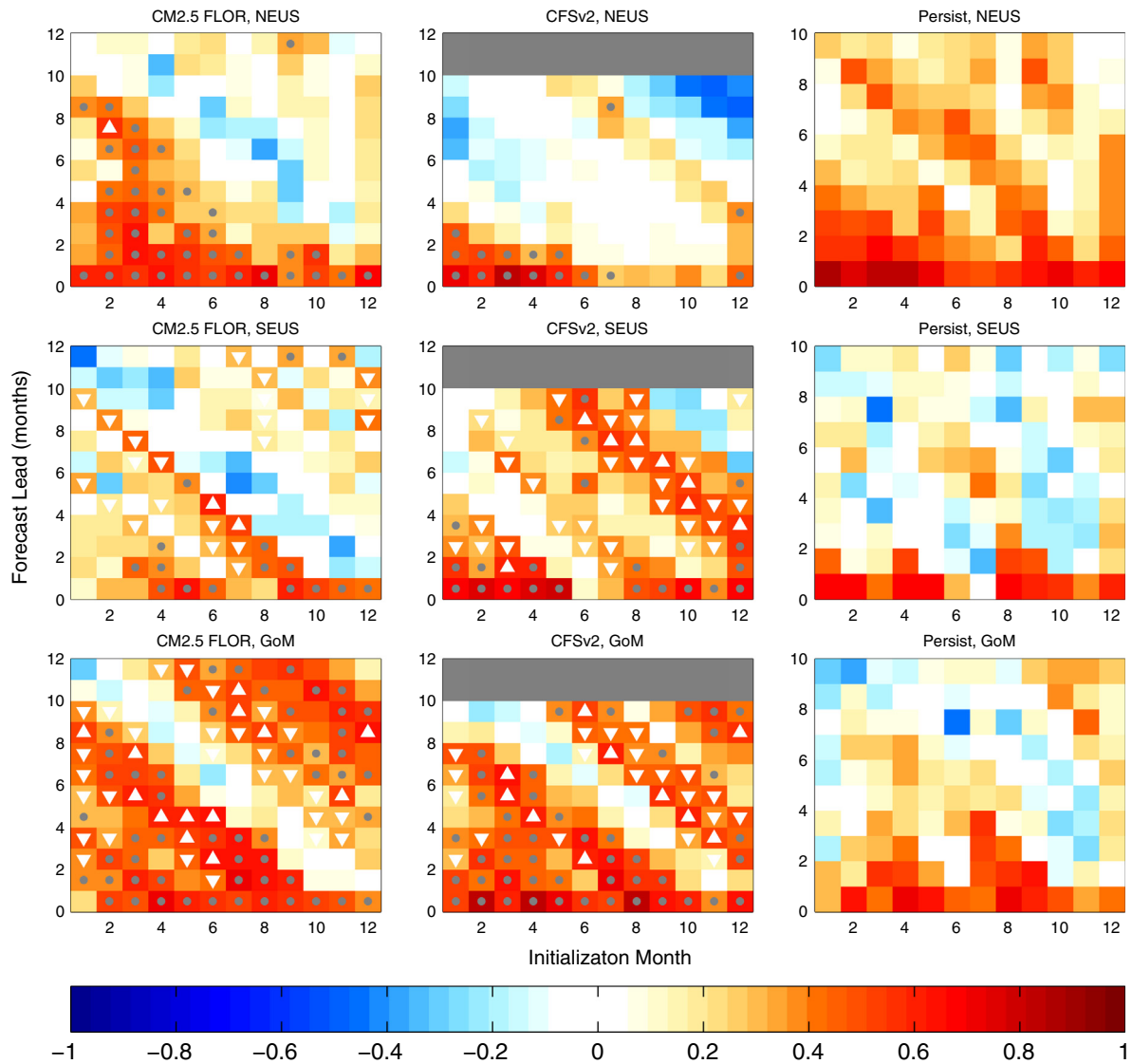
Fig. 3. Anomaly correlation coefficients (ACCs) as a function of forecast initialization month (x-axis) and lead time (y-axis). Notation is as described for Fig. 2.
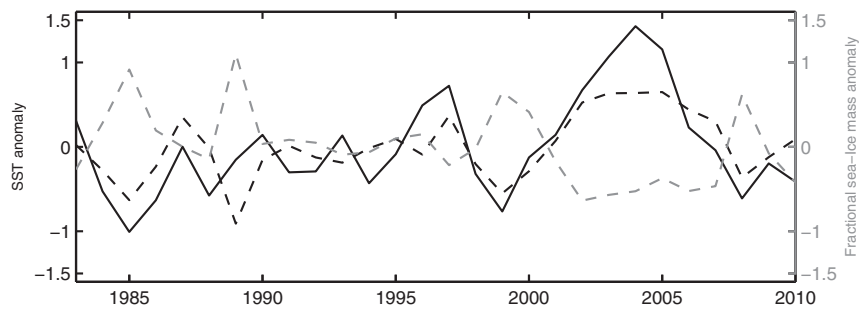

Fig. 4. August initialized prediction of the following May/June/July in CM2.5 FLOR for the EBS LME. The solid black line is the OISST.v2 SST mean May/June/July anomaly. The dashed black line is the model prediction (r = 0.76 between OISST.v2 and predicted). The dashed gray line – corresponding to the right hand axis – is the forecast March sea ice mass anomaly, expressed as a fractional departure from the mean. The correlation between the forecast sea ice mass anomaly and the forecast May/June/July SST anomaly is −0.64. That is, years with low ice mass in the EBS tend to have a warmer May/June/July and those with high ice mass a colder May/June/July.

Gulf of Alaska (GoA) forecasts, particularly those from CM2.5 FLOR, exhibit a prominent diagonal ridge of ACCs > 0.5 and significantly above persistence for February–March (FM) predictions (Fig. 2, row 2). FM GoA anomalies have a strong correlation with basin-scale SST variations (Fig. 5A) that are consistent spatially with anomalies resulting from ENSO and its teleconnections, which

peak in the boreal Fall and Winter (Alexander et al., 2002), and the Pacific Decadal Oscillation (Mantua et al., 1997). Indeed, the correlations of GoA FM SST anomalies with the PDO and Nino3.4 indexes are 0.89 and 0.63, respectively. This tight linkage to basin-scale variability contrasts with late Spring through Fall anomalies which do not exhibit strong linkages with basin-scale climate variations
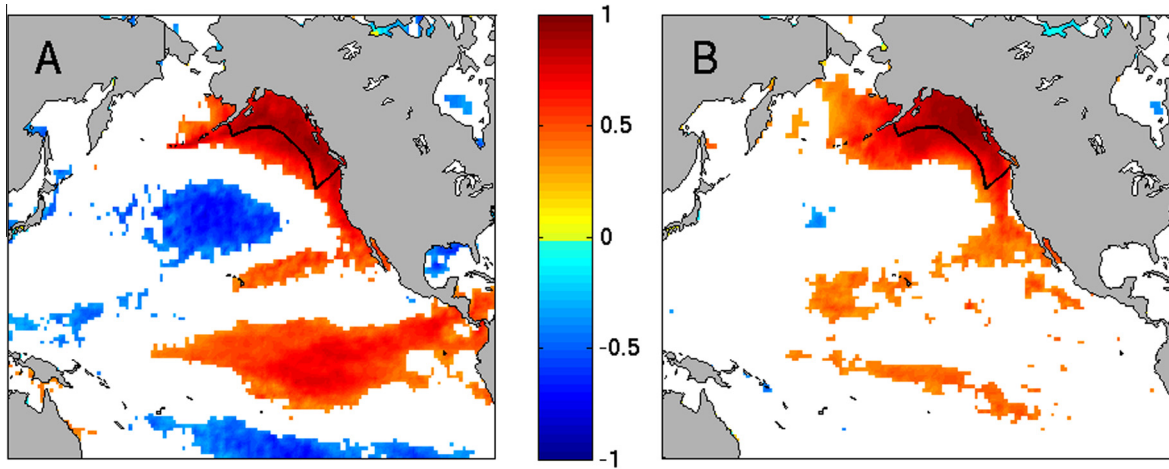
Fig. 5. A: Correlation between the March Gulf of Alaska LME SST anomaly and March SST anomalies over the equatorial and North Pacific (both the LME-average and spatially-resolved anomalies are based on NOAA OISST.v2). Note the strong covariation with basin-scale patterns similar to those associated with ENSO and PDO. B: As in panel (A), but for August when covariation with basin-scale patterns is much weaker. The Gulf of Alaska LME is outlined in black in both panels. Correlations are only shown if they are significantly different than 0 with 95% confidence.

(Fig. 5B, r = 0.38 with the PDO index and r = 0.35 with the Nino3.4 index). CM2.5 FLOR's ability to capture the transition of the GoA from these more "localized" SST anomalies during the late Spring/Fall to SST anomalies with strong links to basin-scale

climate variations in late winter/early spring thus generates the skill above persistence for FM forecasts in the Gulf of Alaska.

Fig. 6 illustrates the mechanisms underlying the transition from localized SST anomalies to anomalies with strong basin-scale
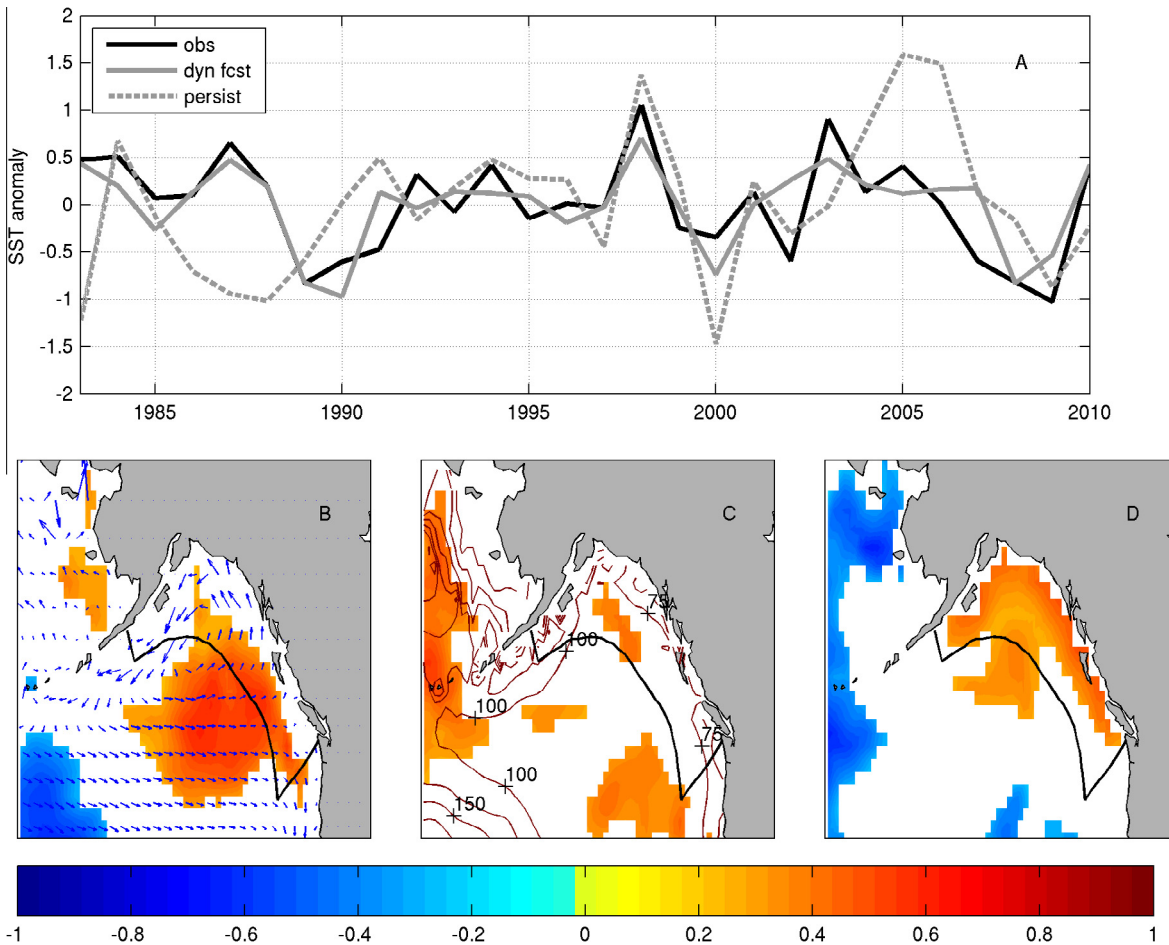

Fig. 6. A: August 1 initialized February–March prediction for the Gulf of Alaska LME SST anomaly in CM2.5 FLOR. The correlation between the model forecast and the reanalysis is 0.75, while the correlation with the persistence forecast is only 0.27. B: Correlation between the August-initialized SST anomaly and the observed February/March SST anomaly; vectors are mean surface currents from August through March subsampled at approximately every 2° Lon/Lat. C: Correlation between August-initialized ocean temperature at 70 m and observed February/March SST anomaly; contours indicate maximum mixed layer depth between the August initialization and the February/March forecast window. D: Correlation between the surface atmosphere to ocean heat flux anomaly (positive into ocean) during and 1 month prior to the February/March forecast window and the observed February/March SST anomaly. In panels (B–D), only correlations that are significant greater than 0 at the 90% confidence level are shown.

linkages in CM2.5 FLOR for an August initialized FM forecast. Improvement over the persistence forecast is clearly evident for this forecast (Fig. 6A; $r = 0.75$ between the dynamical forecast and OISST.v2; $r = 0.27$ between the persistence forecast and OISST.v2). Correlation patterns suggest advection of offshore SST anomalies from the August initialization into the GoA (Fig. 6B) and winter heat flux anomalies (Fig. 6D) as primary drivers of the FM SST anomaly, with emergence of subsurface anomalies playing a lesser role (Fig. 6C). The role of anomalous winter heat fluxes in driving FM SST anomalies in the Gulf of Alaska is consistent with strong southerly winds carrying anomalously warm, moist air over the Gulf of Alaska during positive phases of PDO and ENSO (Alexander et al., 2002; Mantua et al., 1997).

Our results in the GoA are generally consistent with those of Wen et al. (2012) in their earlier evaluation of CFSv2. In particular, Wen et al. (2012) found that 6-month SST predictions for the Gulf of Alaska had the highest mean skill from predictions initialized in August versus other times of year. Moreover, the western Gulf of Alaska was one of the regions where the model had significantly higher skill than persistence in its forecasts with 6-month leads. The prominence of the FM ACC "ridge" in CM2.5 FLOR extends this prior result.

The California Current (CC) LME SST anomaly predictions in CM2.5 FLOR and CFSv2 (Fig. 2, row 3) show a similar ridge of enhanced predictive skill for winter and early spring forecasts as the GoA. February, March, and April ACCs are generally higher than the persistence forecast though, unlike the GoA, they rarely exceed persistence with 90% confidence. Like the GoA, skill is linked to the forecast systems ability to capture transitions between localized SST anomalies from Spring through Fall and basin-scale variability during the winter and early spring (not shown).

Insular Pacific–Hawaiian (IP–H) LME forecasts exhibit high ACC values for both forecast systems across most start months and leads (Fig. 2, row 4). In addition, predictions of winter and spring conditions based on summer through early winter initializations greatly exceed the skill of the persistence forecast. Fig. 7 elucidates the mechanism underlying this skill through the example of a September 1 initialized January–March SST anomaly forecast from CM2.5 FLOR. During September, the IP–H LME lies between two opposing centers of ENSO-linked SST variability in the North Pacific (Fig. 7B). The forecast January–March anomaly, however, shows a strong positive correlation with anomalies to the North and a negative correlation with eastern equatorial anomalies. The boundary between the initialized northern and equatorial anomalies migrates southward through the late summer and into winter, such that the IP–H LME is mostly overlain by the initially northern anomaly by the January–March forecast window (Fig. 7C). The accurate representation of this transition in the dynamical forecast yields a correlation with OISST.v2 of 0.84, far higher than the persistence correlation of 0.02 (Fig. 7A). It is notable, however, that the large Latitudinal extent of the IP–H may lead to differences between the LME-mean anomaly and that experienced at a given Latitude. For instance, much of the Hawaiian chain in Fig. 7C remains Southeast of the northern anomaly even in January–March. This heterogeneity was reflected in lower coherence of SST anomalies within the IP–H LME relative to the others (Table 1).

Both forecast systems are challenged in the smaller LMEs along the U.S. East Coast (Fig. 3, rows 1 and 2). Skill in the Northeast U.S. (NEUS) is low aside from prediction of spring/summer conditions from winter/spring initializations in CM2.5 FLOR. This skill, however, can be primarily attributed to persistence. Performance is better in the Southeast U.S. (SEUS), particularly for CFSv2. Skillful prediction of fall SST anomalies for CFSv2 are linked to the northward propagation of equatorial Atlantic SST anomalies in a manner consistent with fall anomalies in the Gulf of Mexico (see below, Fig. 8). The uncertain reliability of historical SST anomaly estimates

for this LME (Section 3.1, Table 3), however, makes interpretation of this skill ambiguous. Prospects for improving predictions in the NEUS and SEUS will be discussed in Section 4.

In the Gulf of Mexico (GoM) LME, both dynamical forecast systems exhibit skill above persistence for late summer/fall and spring forecasts, but fail to predict winter conditions at most leads. For late summer/fall forecasts, skill is linked to tropical Atlantic SST anomalies. Fig. 8, for example, shows a December-initialized August–September SST anomaly forecast for the GoM LME in CM2.5 FLOR. The correlation between the dynamical forecast and the observations is 0.58 and primarily reflects agreement on a warming trend over the past 30 years (Fig. 8A). Forecast summer/fall anomalies show a clear, positive correlation with winter-initialized low latitude Atlantic SST anomalies (Fig. 8B) that strengthen and propagate into the Gulf of Mexico through the spring (Fig. 8C) and summer (Fig. 8D). The monotonic increase in predicted anomalies suggest a linkage to the Atlantic Meridional Oscillation (AMO, Delworth and Mann, 2000), which exhibited low values in the 1980s and early 1990s before transitioning to and maintaining higher values from mid-1990s (e.g., Deser et al., 2010). It is notable that the equatorial Atlantic linkages illustrated in Fig. 8 also yield considerable prediction skill in the Caribbean Sea and Northern Brazil for both models (see Supporting material) and, in CFSv2, suggests a mechanism for fall predictability in the SEUS LME.

Spring forecast skill in the Gulf of Mexico is linked to the tropical Pacific variability (Fig. 9B), with cool/warm springs following 1 year after an El-Nino/La-Nina event (Fig. 9A, note cold anomalies after strong El-Nino's in 1982, 1987, 1992, and 1997; warm anomalies following strong La Ninas in 1985, 1989, 1999/2000, and 2008). The pattern is explained by ENSO teleconnections driving winter heat flux anomalies within the Gulf of Mexico (Fig. 9C, Alexander et al., 2002). Predictive skill through this mechanism is moderate ($r = 0.57$ between the forecast and OISST.v2 in Fig. 9A), suggesting the presence of significant other sources of variability not captured by the prediction.

3.3. Exploring SST anomaly prediction across global LMEs

Detailed examination of seasonal prediction in U.S. LME's provided a spectrum of prediction success and highlighted several mechanisms for generating skill above persistence. Predictability assessments for 66 LMEs globally for both the CM2.5 FLOR and CFSv2 forecasts are provided in the Supporting material and expand the scope of this limited U.S. sample. We highlight several additional cases of notable skill above persistence from this wider set of LMEs as regions with high potential for marine resource applications, while noting that additional scrutiny relative to local datasets is needed to confirm skill (e.g., Section 3.1) and mechanistic investigation to gain more detailed understanding of the processes responsible for skill above persistence (e.g., Section 3.2) would improve confidence in applications.

Chief among the mechanisms leading to skill above persistence in U.S. LMEs analyzed in Section 3.2 were (a) alternation between "localized" SST variations not predicted by global forecast systems and the emergence of predictable signals associated with basin-scale climate variability (e.g., Fig. 5, GoA, CC, GoM examples), and (b) the predictable evolution of basin-scale climate modes within an LME (e.g., Fig. 7, IP–H). It is thus not surprising that equatorial LMEs directly impacted by ENSO, such as those in the western tropical Pacific (Fig. 10), are amongst those exhibiting forecasts with the highest skill above persistence. Other equatorial LMEs (see Supporting material) with notable predictability above persistence include the Indian Ocean (Agulhas and Somali Currents, the Arabian Sea, the Bay of Bengal), the Pacific Central American LME (at the eastern end of the ENSO signal), and West African LMEs
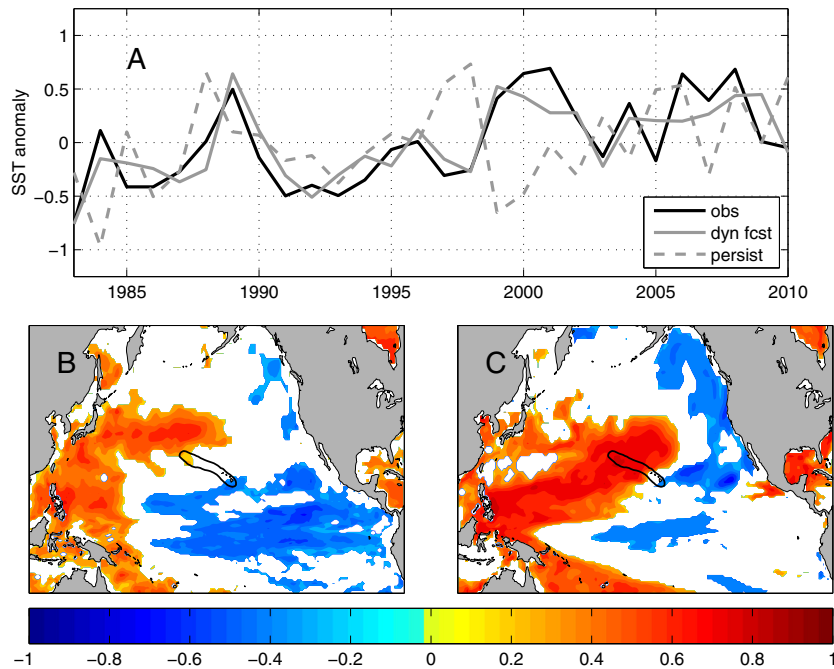
Fig. 7. A: September 1 initialized January–March SST anomaly forecast for the Insular Pacific–Hawaiian (IP–H) LME in CM2.5 FLOR. The correlation between the dynamical forecast and January–March OISST.v2 in 0.84; the correlation between the persistence forecast and OISST.v2 is 0.02. B: Correlation between the September 1 initialized SST anomaly and the January–March NOAA OISST.v2 IP–H LME SST anomaly. C: Correlation between the spatially-resolved February SST anomaly forecast and the OISST.v2 January–March IP–H LME SST anomaly. Note the southward migration of the central north Pacific anomaly over the IP–H region. In panels (B and C), only correlations that significantly exceed 0 with 90% confidence are shown.
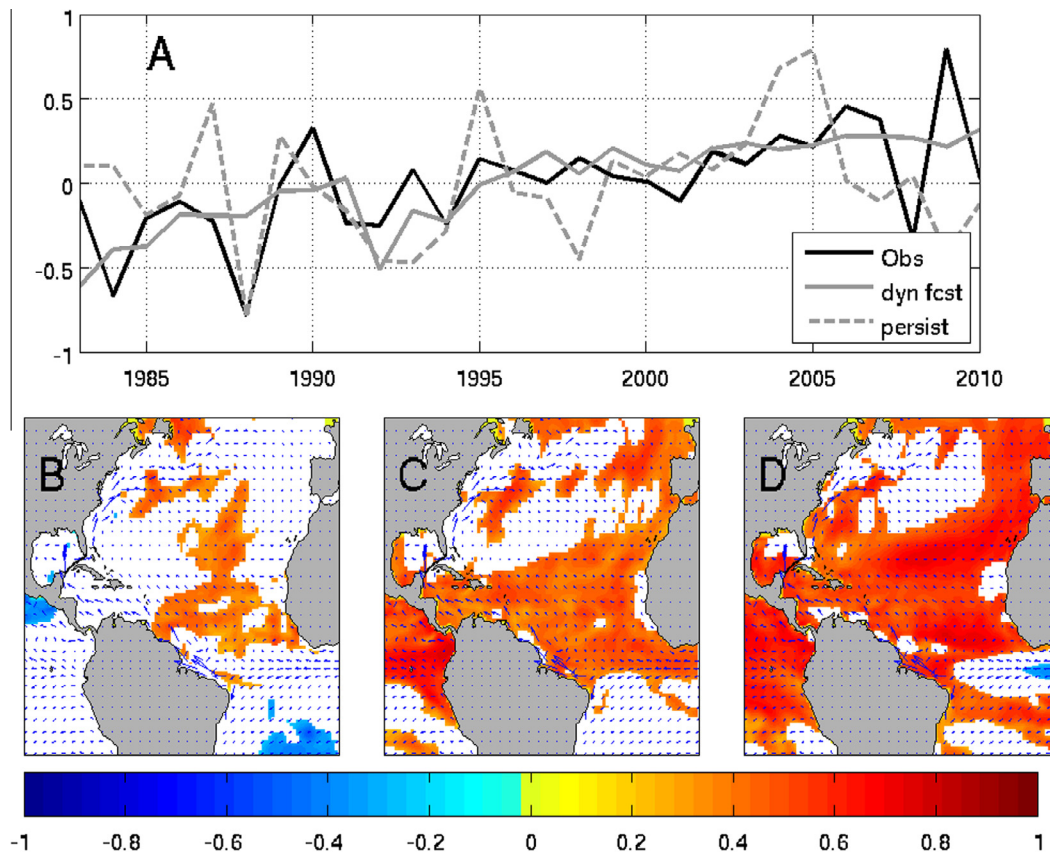

Fig. 8. A: December initialized August–September SST anomaly forecast for the Gulf of Mexico LME in CM2.5 FLOR. The correlation between the dynamical forecast and OISST.v2 in 0.57; the correlation between the persistence forecast and OISST.v2 is 0.21. Panels B–D: the progression of the spatially resolved covariance between SST over the North Atlantic Basin and the GoM August to September SST anomaly over the course of the forecast. B: Correlation between the December-initialized SST anomaly and the OISST.v2 August–September Gulf of Mexico LME SST anomaly. C: Correlation between the spatially resolved May SST anomaly forecast and the OISST.v2 August–September Gulf of Mexico LME SST anomaly. D: Correlation between the spatially resolved August SST anomaly forecast and the OISST.v2 August–September Gulf of Mexico LME SST anomaly. Vectors in all panels are mean December–August surface currents sub-sampled at ~2° Lat/Lon and only correlations that significantly exceed 0 with 90% confidence are shown.
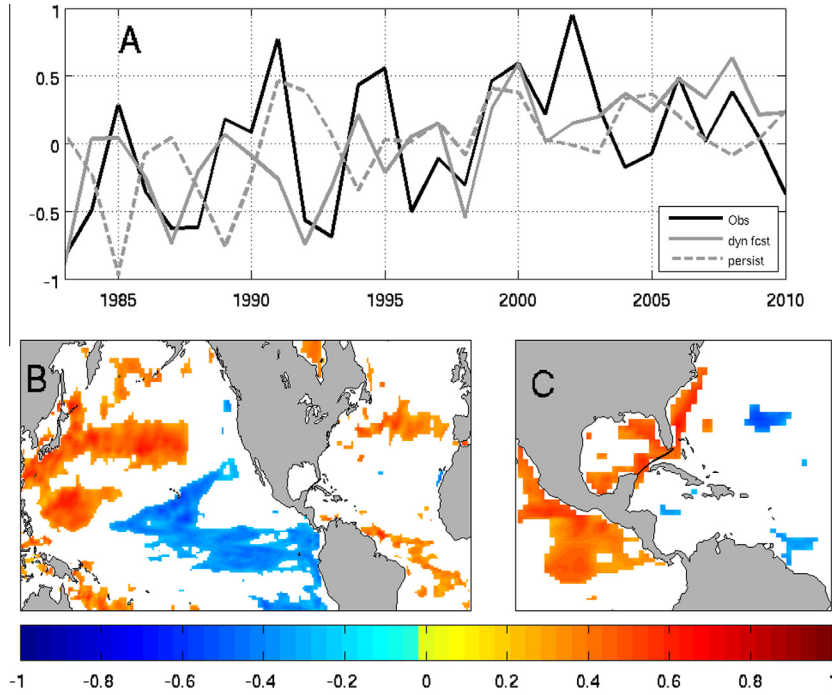
Fig. 9. A: July initialized April–May SST anomaly forecast for the Gulf of Mexico LME in GFDL-FLOR. The correlation of the dynamical forecast and OISST.v2 is 0.58; the correlation between the persistence forecast and OISST.v2 is 0.02. B: Correlation between the initialized SST anomaly and the OISST.v2 April–May Gulf of Mexico LME SST anomaly. C: Correlation between the July initialized November through December heat flux anomaly and the OISST.v2 April–May Gulf of Mexico SST anomaly. In all cases, only correlations that significantly exceed 0 with 90% confidence are shown.
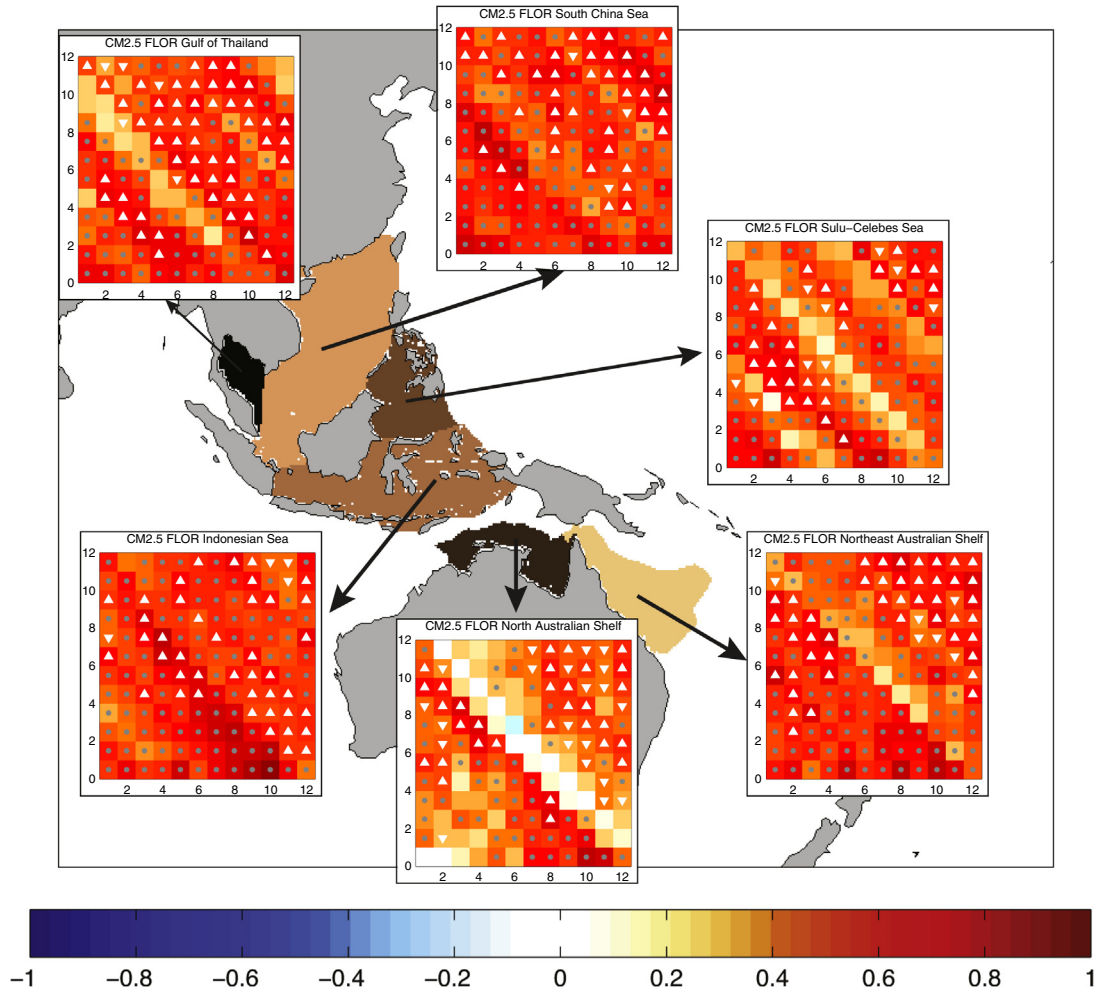

Fig. 10. CM2.5 FLOR predictions for western tropical Pacific LMEs. Grids are as in Fig. 2.
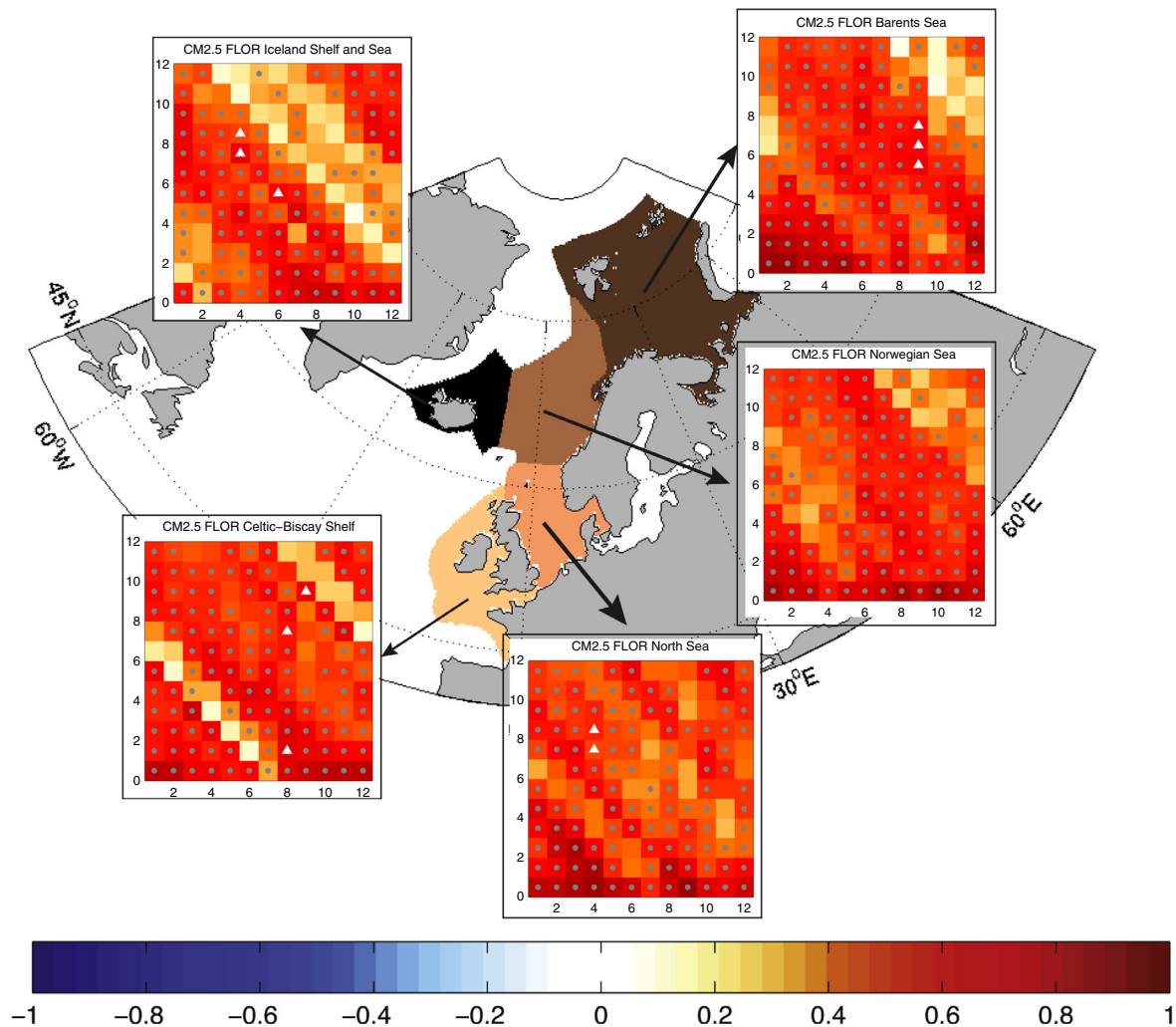
Fig. 11. CM2.5 FLOR predictions for Northeast Atlantic LMEs. Grids are as in Fig. 2.

impacted by the Atlantic Nino (Guinea Current extending southward into the Benguela).

In the extratropics, the Northeast Atlantic LMEs exhibit high ACCs across a range of initialization months and leads (Fig. 11). Skill, however, rarely exceeds that of the persistence at the 90% level. This reflects the predominance of low-frequency basin-scale climate variability in the Northeast Atlantic, which minimizes both seasonal local/basin-scale contrasts and the degrees of freedom within the retrospective forecasts. It is important to note, however, that while skill above persistence is a critical metric for assessing dynamical forecast systems, it is not necessarily a prerequisite for the utility of predictions for marine resource applications. Skill above persistence may also arise within Northeast Atlantic LMEs with longer times series, by considering more coastal sub-regions, or with improved resolution of local scale processes that create distinctions from basin-scale dynamics (see Section 4).

The seasonal cycle of mixed layer depth in the extratropical oceans has the potential to influence the evolution of SST anomalies and thus their predictability. Temperature anomalies that form at the surface due to anomalous surface heat fluxes in winter, spread throughout the deep winter mixed layer, are sequestered beneath the mixed layer when it shoals in spring, remain intact in summer and are then re-entrained into the surface layer in the subsequent fall and winter. The SST anomalies in the shallow mixed layer during the intervening summer are strongly damped by surface heat fluxes. This process leads to the winter-to-winter reemergence of SST anomalies in portions of the Atlantic and Pacific and Oceans (Alexander et al., 1999; Hanawa and Sugimoto, 2004; Namais and Born, 1970, 1974). Forecast skill due to reemergence in both the model and SST persistence forecasts will be indicated by higher correlations from winter/spring to the following fall/winter (lags of 6–12 months) with a drop in correlations during the summer, as appears to be the case for the Sea of Japan/East Sea LME (Fig. 12). Model forecasts initialized in summer can provide skill above SST persistence as they include temperature anomalies located below the mixed layer in the summer seasonal thermocline (approximately 20–100 m) that return to the surface in the fall and winter. Extensions of the reemergence paradigm: (i) that anomalies can propagate from where they were initiated to where they return to the surface ("remote reemergence" – de Coetlogon and Frankignoul, 2003; Sugimoto and Hanawa, 2007) and (ii) the temperature anomalies may be due to ocean heat advection (rather than mixing) that extends to the surface in winter but is covered over by a shallow mixed layer in summer, may also produce skill above persistence in extratropical regions.

Lastly, the East Bering Sea (EBS) analysis in Section 3.2 suggested that accurate initiation of sea-ice mass anomalies may generate skill above persistence for winter initialized SST anomaly predictions of the following Spring and Summer. Hints of this
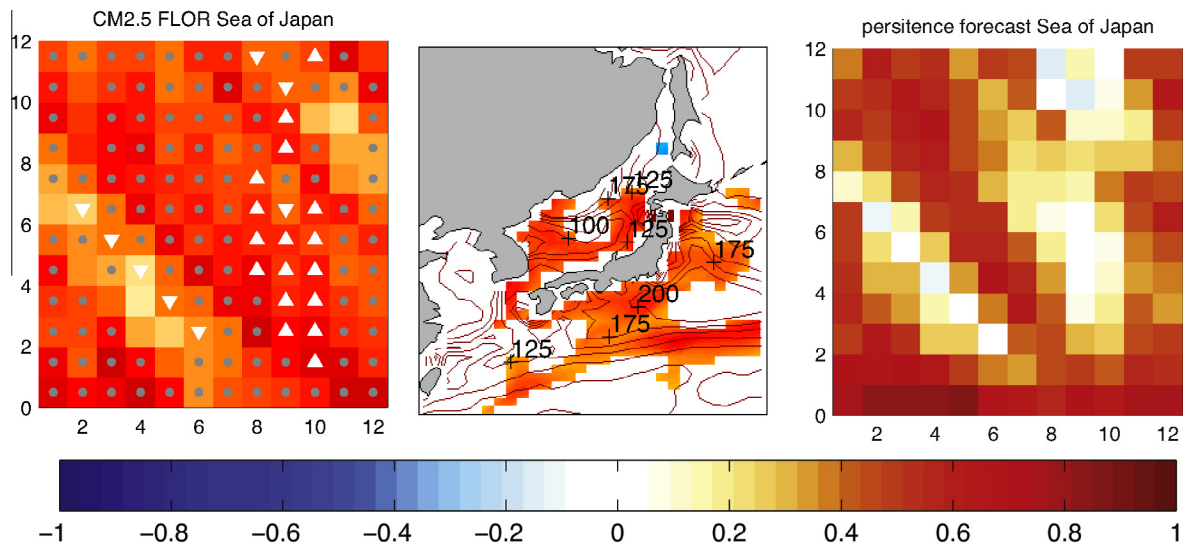
Fig. 12. Left: Winter re-emergence of SST anomalies in the Sea of Japan. Left panel: Forecast ACC as a function of initialization (*x*-axis) and forecast lead (*y*-axis) for CM2.5 FLOR in the Sea of Japan. Middle: Correlation between the September initialized 75 m temperature anomaly and forecast anomalies in December-February. Only correlations that are greater than 0 with 90% confidence are shown. Right: As in left panel, but for persistence. Grid is as in Fig. 2.

mechanism are apparent in the Arctic, particularly the Beaufort, Chukchi, and East Siberian Seas (Fig. 13). The potential of this mechanism to generate skillful SST anomaly predictions suggests closer scrutiny and improvement of sea ice mass initializations.

4. Discussion

The SST anomaly prediction skill, as measured by the ACC, varied greatly by LME, initialization month, and lead. The frequency of skillful predictions arising through a diversity of mechanisms, however, suggests considerable potential utility of global dynamical climate forecast systems for LME-scale SST prediction and subsequent application to marine resources. We now further discuss the strengths, limitations, and priority developments of global seasonal forecast systems for such applications, before offering some concluding remarks on marine resource management applications.

Accurate, continuous estimates of past variations in ocean state at the scales of interest are a critical prerequisite for establishing forecast skill. Detailed assessment of OISST.v2 anomaly estimates (Reynolds et al., 2007) against point-wise in-situ observations (Boyer et al., 2013) supported the general robustness of OISST.v2 for LME-scale SST variability. Disagreement in the SEUS LME, however, suggests room for further improvement and underlines the need for careful scrutiny of ocean and climate reanalyses at the scales of interest before accepting them as "observations". Continued maintenance of and advances in ocean observing systems (e.g., GCOS, 2010; IOOS, 2013) are essential for improving observational constraints for both the initiation and assessment of predictions. While the success of OISST.v2 at the LME-scale is encouraging, SST's are amongst the most extensively observed ocean variables via both in-situ and remote means. Other ecologically-relevant ocean variables, such as sea surface salinity (SSS) or bottom temperature, have far fewer constraints. The prediction "bottleneck" for many ecologically relevant variables thus begins with accurate retrospective estimates.

We assessed the consistency SSS anomalies for several global ocean data assimilation products at the LME-scale and found far less agreement (Table 5). The CFSR system, whose ocean assimilation is based on the Global Ocean Data Assimilation System (GODAS, Xue et al., 2011) includes strong damping to

climatological World Ocean Atlas salinity fields at the surface and assimilation to climatological Temperature–Salinity relationships at depth. It thus does not capture seasonal salinity anomalies. GFDL's ECDA system (Zhang et al., 2007) and the Simple Ocean Data Assimilation (SODA, Carton and Giese, 2008) were able to match relatively small SSS deviations in oceanic systems fairly well (Table 5, IP–H, CC LMEs) but coastal regions subject to stronger riverine SSS variations generally exhibited lower correlations and significant biases. SSS anomalies are also more heterogenous within LMEs. Detailed inspection of correlations spatially (not shown) suggests poor skill in near-shore regions that often improves offshore. In the case of SSS, the Aquarius satellite (Lagerloef et al., 2008) may provide improved anomaly constraints if time-series are sustained and bias issues for coastal regions can be overcome.

We also reiterate that the impacts of SST (and SSS) on species of interest are often indirect (Section 1). That is, SST and SSS often do not drive ecosystem change through direct physiological effects, but serve as a proxy for other system characteristics (e.g., mixed layer depth, stratification, horizontal transports, etc.) actually driving ecosystem changes. Such proxy relationships can break down (Myers, 1998), providing impetus for direct prediction of driving properties (e.g., Hobday and Hartog, 2014). The sub-surface information required to assess predictions of subsurface ecosystem properties are scanty in most coastal zones, but there are selected locations where extended time series of vertical ocean profiles are available (McClatchie et al., 2014). In the northeast Pacific, for example, time series are available for the Seward line in the GOA (e.g., Weingartner et al., 2005), the Newport line off the Oregon coast (e.g., Peterson et al., 2002), and from the CalCOFI program for southern California (Pena and Bograd, 2007). For bottom temperatures, fisheries surveys provide systematic, controlled observations for select seasons in many ecosystems globally (e.g., Pinsky et al., 2013). Future efforts to assess predictions against these data sources are needed.

SST anomaly prediction skill varied widely by LME. The Northeast and Southeast U.S. (NEUS, SEUS) LMEs posed perhaps the largest challenge for global dynamical forecast systems of the seven considered in detail. These LMEs are amongst the smallest globally. They are also adjacent to an energetic western boundary current which is too laminar at the coarse ocean resolution used by
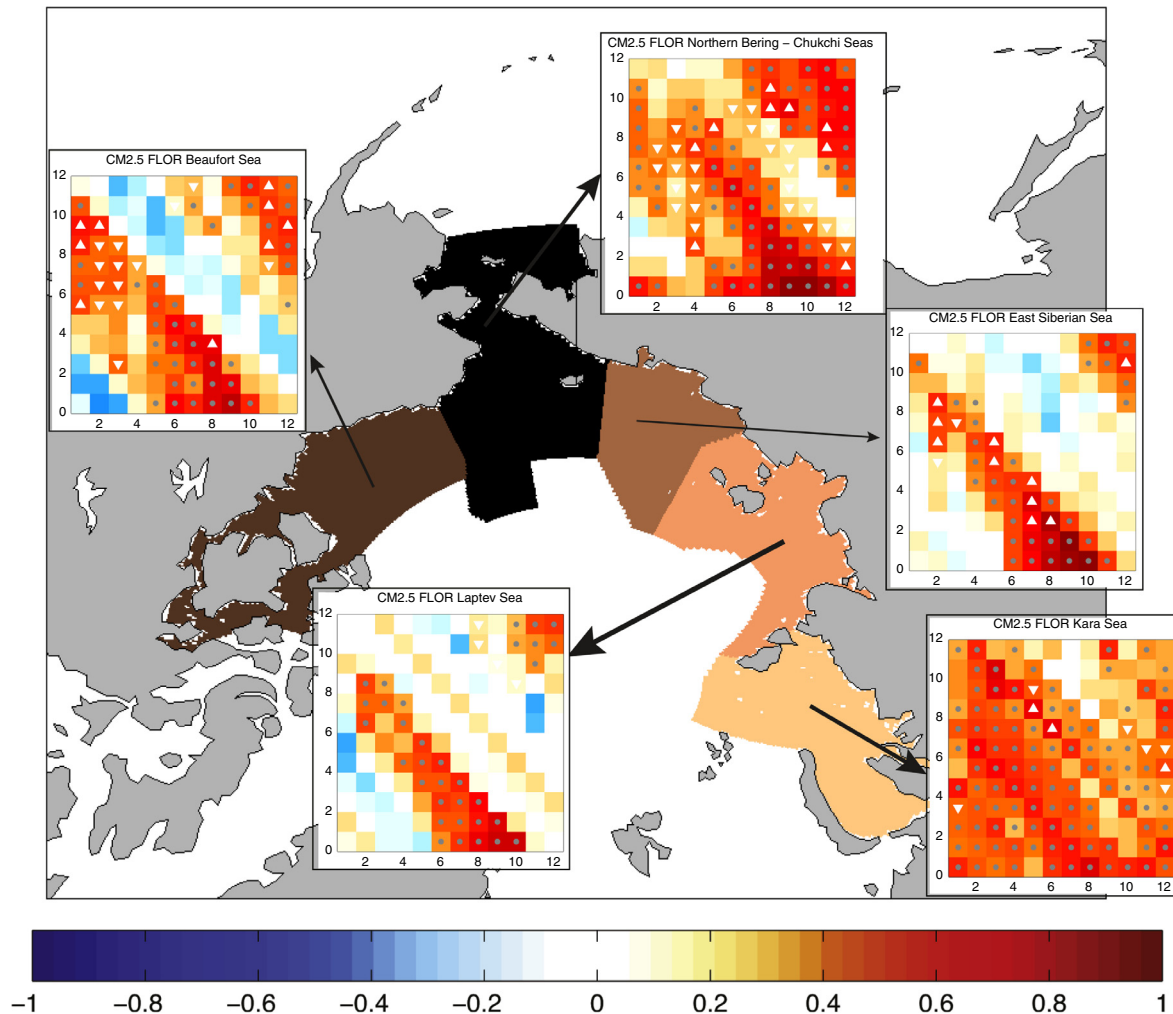
Fig. 13. SST anomaly predictions in the Arctic in CM2.5 FLOR. Grids are as in Fig. 2.

Table 5
A comparison of LME-scale seasonal salinity anomalies from the GFDL ECDA (reference) and SODA 2.2.4 reanalyses (reference) against WOD13 SSS observations via the methodology described in Section 2.2, but using the respective ODAs as reference climatologies rather than OISST.v2. The comparison considers the years 1982 through 2010, a period common to the reanalyses and covering most of the hindcast period. SSS observations <25 PSU, generally a small fraction of points, were omitted from the comparison to minimize estuarine influence. This did not significantly effect the overall poor agreement between WOD13-based SSS anomalies and the reanalyses. SSS anomalies in the CFSR and GODAS reanalyses (not shown) were both strongly damped to climatologies and are not shown.

	EBS	GoA	CC	IP–H	GoM	SEUS	NEUS
GFDL-WOD							
r	0.63	0.01	0.68	0.76	0.12	0.47	0.35
Bias/$4\sigma_w$	0.14	0.29	0.02	0.07	0.27	0.16	0.29
σ_{ECDA}/σ_w	0.55	0.33	0.82	0.87	0.40	0.48	0.91
SODA-WOD							
r	0.45	0.04	0.80	0.78	0.18	0.26	0.66
Bias/$4\sigma_w$	0.15	−0.01	0.07	0.06	0.28	0.28	0.14
σ_{SODA}/σ_w	0.63	0.33	0.99	0.89	0.18	0.25	0.73

global forecast systems, contributing to biases in the separation point between the Gulf Stream and the eastern U.S. continental shelf and in the subsequent Gulf Stream path (e.g., Delworth et al., 2012). The Gulf Stream position has been shown to influence water masses in both the NEUS and SEUS LMEs by controlling water flow through deep channels along the shelf-break not

resolved by 50–100 km resolution (Drinkwater et al., 2003; Pershing et al., 2001) with subsequent effects on fish populations (Nye et al., 2011). Furthermore, poorly-resolved southward flowing coastal currents provide key transport pathways from maritime Canada and the Arctic (Chapman and Beardsley, 1989; Fratantoni and Pickart, 2007; Loder et al., 1998). Finer ocean resolution is thus likely to be a key improvement for SST prediction in the NEUS and SEUS LMEs. With improved resolution of the processes connecting the ocean basin to the shelf, the diversity of large-scale climate drivers of shelf variability in the NEUS and SEUS raises the potential for considerable prediction skill. Empirical forecasts linking basin-scale properties to lagged shelf-scale responses in these regions (e.g., Greene and Pershing, 2003) may provide a means for progress as dynamical systems are refined. Such statistical approaches rely on the stationarity, but they are often competitive with dynamical forecasts in seasonal climate and ENSO prediction (e.g., Barnston et al., 2012). As with dynamical forecasts, however, most past statistical prediction studies focus on basin-scale modes of variation (e.g., Alexander et al., 2008; Hawkins et al., 2011; Newman, 2007).

While improved ocean resolution may be important for the NEUS and SEUS, the atmosphere plays the central role in resolving basin-scale patterns of ocean variability (e.g., Alexander et al., 2002; Deser et al., 2010) underlying many instances of skill above persistence. Likewise, deficiencies in atmospheric models contribute to ocean biases commonly attributed to poorly-resolved

ocean dynamics. Misplaced westerlies and subsequent biases in wind stress curl, for example, contribute to errors in western boundary current positions (e.g., Kwon et al., 2010). Insufficient wind stress and over-estimation of insolation due to cloud biases contribute to warm biases in eastern boundary current upwelling regions (Large and Danabasoglu, 2006). Continued improvement in atmospheric resolution and dynamics is thus also essential to SST forecast improvement. A tangible illustration of this is provided by improved SST predictions in western tropical Pacific LMEs in CM2.5 FLOR (Fig. 10) relative to those in GFDL's CM2.1 prediction system (Fig. 14). CM2.1 features the same ocean resolution and ocean initialization as CM2.5 FLOR but has much coarser atmospheric resolution (∼200 km compared with ∼50 km in CM2.5 FLOR). The improvement for western tropical Pacific SST anomaly prediction in CM2.5 FLOR is indicative of improved equatorial Pacific climate dynamics in CM2.5 FLOR that accompany the enhanced atmospheric resolution in this model (Jia et al., 2015).

Results from the East Bering and Chukchi Sea LMEs highlight the potential value of improved sea-ice initialization to SST anomaly predictions for the following spring and summer. It is notable, however, that spring/summer predictions were often better for forecasts initialized in fall and spanning winter months than for those initialized in winter (i.e., Fig. 2, row 1; Fig. 13). This suggests that the forecast system may be better at dynamically simulating the emergence of EBS winter ice mass anomalies based on fall

initializations than initializing them directly. Improved initialization of sea-ice thickness and extent, a priority for Arctic ice prediction (Guemas et al., 2014; Msadek et al., 2014; Wang et al., 2013) may thus also benefit SST anomaly prediction.

A final potential means of enhancing forecast skill is the use of multi-model ensembles. The mean of a multi-model ensemble has been shown to perform better than individual models for some quantities over diverse spatial and temporal scales (e.g., Kirtman et al., 2014; Reichler and Kim, 2008). Such ensembles can include statistical and dynamical approaches (Barnston et al., 2012). A full exploration of the value of ensemble approaches for SST anomaly prediction across the range of systems explored herein is beyond the scope of this contribution and is left to future work in system specific contexts.

5. Prospects for marine resource applications

We end with some remarks on the potential value of coastal SST anomaly forecasts for marine resource applications. Significant, mechanistically-motivated relationships between ocean temperature and marine resource responses are common (Section 1) and seasonal SST forecasts have already proven useful for a number of marine resource applications (Hobday et al., 2011; Spillman et al., 2013; Spillman and Hobday, 2014). Skillful SST anomaly predictions at marine-resource relevant scales have the potential to
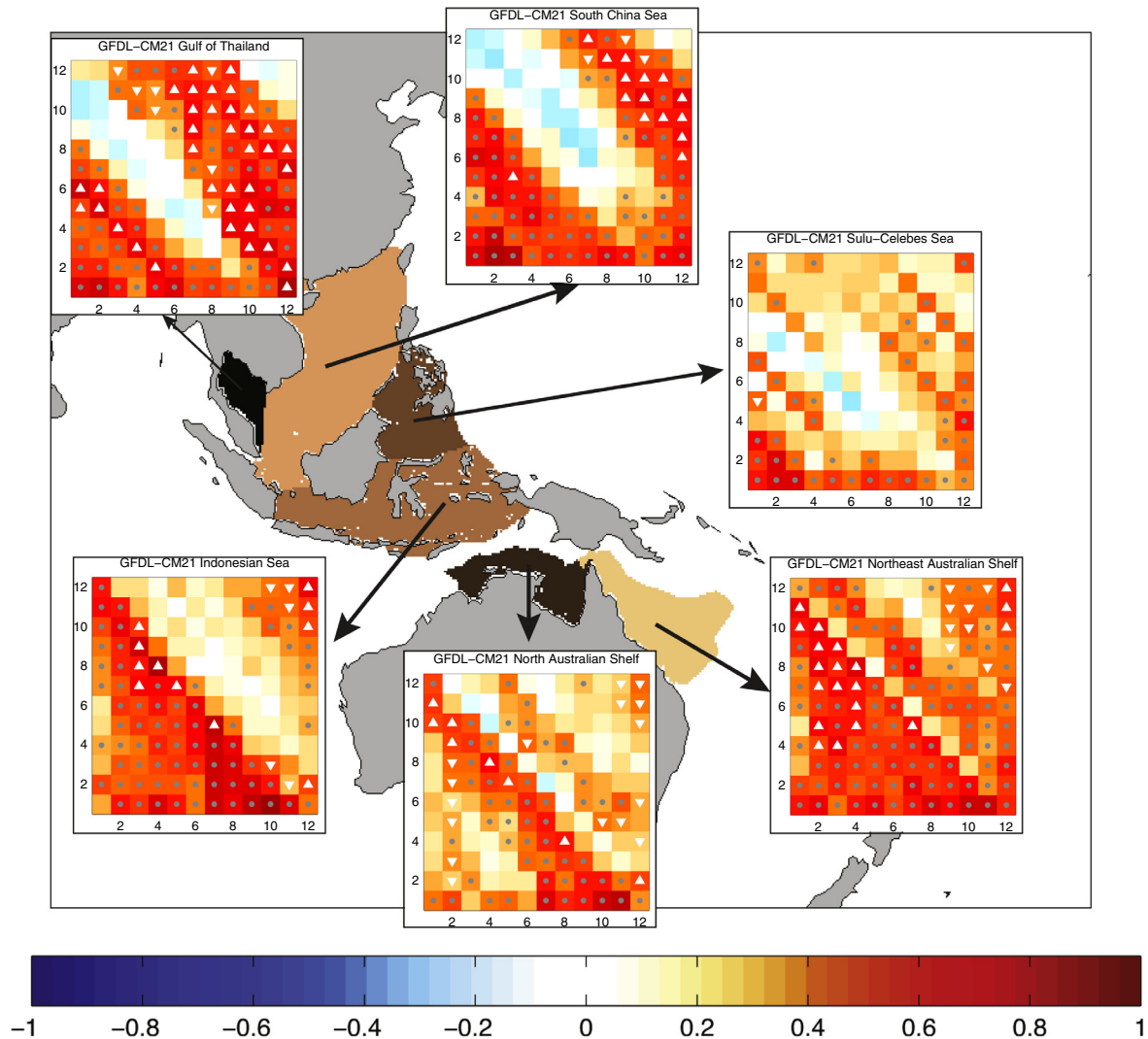

Fig. 14. GDL CM2.1 predictions for the western tropical Pacific/Eastern Indian Ocean. Grids are as in Fig. 2.

broadly support more effective and proactive dynamic management strategies for marine resources (Hobday et al., 2014; Pinsky and Mantua, 2014) by enabling anticipatory rather than reactive marine resource management. While skill above persistence is desirable for such applications, it is not required. Persistence skill alone still improves upon the common implicit assumption that the future environment is equally likely to be any one from the full range of past states. The numerous cases herein of high SST anomaly prediction skill that does not exceed persistence should thus not be discounted for potential marine resource applications.

Successful application of global climate forecasts within marine resource management, however, requires more than just skillful environmental forecasts. Current fisheries harvest control rules, for example, rely on short-term stock biomass projections based on past and present estimates of factors, such as recruitment deviations, catchability, and body growth that are allowed to fluctuate randomly according to past distributional information (Methot, 2009; Walters, 1989). Potentially prominent environmental effects (e.g., Maunder and Watters, 2001; Mueter et al., 2009; Szuwalski et al., 2013; Vert-pre et al., 2013) are often encompassed within unexplained variability (Quinn and Deriso, 1999; Walters and Martell, 2004), contributing to sub-optimal management (Keyl and Wolff, 2008). Understanding the relationships between predictable environmental drivers and marine resource responses (Myers, 1998) and integration of these relationships into management frameworks are essential pre-requisites to forecast applications. This holds for forecast applications across the marine resource management spectrum (e.g., distributional prediction for spatial zoning, by-catch avoidance, sampling-observer designs). Regardless of the context, careful scrutiny of the risks and benefits of such integrated frameworks via management strategy evaluation (A'mar et al., 2009; Haltuch et al., 2009; Punt et al., 2014; Szuwalski and Punt, 2013) are also desirable prior to operational use.

While successful application of monthly to inter-annual climate forecasts to marine resource management is a multifaceted challenge, results herein suggest that the time is ripe for concerted investigation of case studies – at least those where LME-scale SST anomalies can serve as a robust driver of marine resource responses. The methodology also provides an approach for assessing predictions of other marine resource relevant drivers across spatial and temporal scales. Expanding efforts in these areas should help realize the value of future information provided by existing monthly to inter-annual forecast systems for management and identify priorities for further development.

Acknowledgements

Appendix A. Supplementary material

Supplementary data associated with this article can be found, in the online version, at http://dx.doi.org/10.1016/j.pocean.2015.06.007.

References

Alexander, M.A., Deser, C., Timlin, M.S., 1999. The reemergence of SST anomalies in the North Pacific Ocean. Journal of Climate 12, 2419–2433.
Alexander, M.A., Blade, I., Newman, M., Lanzante, J.R., Lau, N.C., Scott, J.D., 2002. The atmospheric bridge: the influence of ENSO teleconnections on air-sea interaction over the global oceans. Journal of Climate 15, 2205–2231.
Alexander, M.A., Matrosova, L., Penland, C., Scott, J.D., Chang, P., 2008. Forecasting Pacific SSTs: linear inverse model predictions of the PDO. Journal of Climate 21, 385–402.
A'mar, Z.T., Punt, A.E., Dorn, M.W., 2009. The evaluation of two management strategies for the Gulf of Alaska walleye pollock fishery under climate change. Ices Journal of Marine Science 66, 1614–1632.
Barnett, T.P., Preisendorfer, R., 1987. Origins and levels of monthly and seasonal forecast skill for United-States surface air temperatures determined by canonical correlation-analysis. Monthly Weather Review 115, 1825–1850.
Barnston, A.G., Tippett, M.K., L'Heureux, M.L., Li, S.H., DeWitt, D.G., 2012. Skill of real-time seasonal Enso model predictions during 2002–11 is our capability increasing? Bulletin of the American Meteorological Society 93, 631–651.
Barton, A.D., Casey, K.S., 2005. Climatological context for large-scale coral bleaching. Coral Reefs 24, 536–554.
Battisti, D.S., Hirst, A.C., 1989. Interannual variability in a tropical atmosphere ocean model – influence of the basic state, ocean geometry and nonlinearity. Journal of the Atmospheric Sciences 46, 1687–1712.
Beaugrand, G., 2003. Long-term changes in copepod abundance and diversity in the north-east Atlantic in relation to fluctuations in the hydroclimatic environment. Fisheries Oceanography 12, 270–283.
Benthuysen, J., Feng, M., Zhong, L.J., 2014. Spatial patterns of warming off Western Australia during the 2011 Ningaloo Nino: quantifying impacts of remote and local forcing. Continental Shelf Research 91, 232–246.
Bjerknes, J., 1969. Atmospheric teleconnections from the equatorial Pacific. Monthly Weather Review 97, 163–172.
Blanchard-Wrigglesworth, E., Armour, K.C., Bitz, C.M., DeWeaver, E., 2011. Persistence and inherent predictability of Arctic sea ice in a GCM ensemble and observations. Journal of Climate 24, 231–250.
Boyer, T.P., Antonov, J.I., Baranova, O.K., Coleman, C., Garcia, H.E., Grodsky, A., Johnson, D.R., Locarnini, R.A., Mishonov, A.V., O'Brien, T.D., Paver, C.R., Reagan, J.R., Seidov, D., Smolyar, I.V., Zweng, M.M., 2013. World ocean database 2013. In: Levitus, S., Mishonov, A. (Eds.), NOAA Atlas NESDIS, vol. 72. NOAA, Silver Spring.
Bretherton, C.S., Widmann, M., Dymnikov, V.P., Wallace, J.M., Blade, I., 1999. The effective number of spatial degrees of freedom of a time-varying field. Journal of Climate 12, 1990–2009.
Carton, J.A., Giese, B.S., 2008. A reanalysis of ocean climate using Simple Ocean Data Assimilation (SODA). Monthly Weather Review 136, 2999–3017.
Chapman, D.C., Beardsley, R.C., 1989. On the origin of shelf water in the Middle Atlantic Bight. Journal of Physical Oceanography 19, 384–391.
Chelton, D.B., Wentz, F.J., 2005. Global microwave satellite observations of sea surface temperature for numerical weather prediction and climate research. Bulletin of the American Meteorological Society 86, 1097.
de Coetlogon, G., Frankignoul, C., 2003. The persistence of winter sea surface temperature in the North Atlantic. Journal of Climate 16, 1364–1377.
Delworth, T.L., Mann, M.E., 2000. Observed and simulated multidecadal variability in the Northern Hemisphere. Climate Dynamics 16, 661–676.
Delworth, T.L., Broccoli, A.J., Rosati, A., Stouffer, R.J., Balaji, V., Beesley, J.A., Cooke, W.F., Dixon, K.W., Dunne, J., Dunne, K.A., Durachta, J.W., Findell, K.L., Ginoux, P., Gnanadesikan, A., Gordon, C.T., Griffies, S.M., Gudgel, R., Harrison, M.J., Held, I.M., Hemler, R.S., Horowitz, L.W., Klein, S.A., Knutson, T.R., Kushner, P.J., Langenhorst, A.R., Lee, H., Lin, S., Lu, J., Malyshev, S.L., Milly, P.C.D., Ramaswamy, V., Russell, J., Schwarzkopf, M.D., Shevliakova, E., Sirutis, J.J., Spelman, M.J., Stern, W.F., Winton, M., Wittenberg, A.T., Wyman, B., Zeng, F., Zhang, R., 2006. GFDL's CM2 global coupled climate models. Part I: formulation and simulation characteristics. Journal of Climate 19, 643–674.
Delworth, T.L., Rosati, A., Anderson, W., Adcroft, A.J., Balaji, V., Benson, R., Dixon, K., Griffies, S.M., Lee, H.C., Pacanowski, R.C., Vecchi, G.A., Wittenberg, A.T., Zeng, F.R., Zhang, R., 2012. Simulated climate and climate change in the GFDL CM2.5 high-resolution coupled climate model. Journal of Climate 25, 2755–2781.
Deser, C., Alexander, M.A., Xie, S.P., Phillips, A.S., 2010. Sea surface temperature variability: patterns and mechanisms. Annual Review of Marine Science 2, 115–143.
Drinkwater, K.F., Petrie, B., Smith, P.C., 2003. Climate variability on the Scotian Shelf during the 1990s. ICES Marine Science Symposia 219, 40–49.
Drinkwater, K.F., Beaugrand, G., Kaeriyama, M., Kim, S., Ottersen, G., Perry, R.I., Portner, H.O., Polovina, J.J., Takasuka, A., 2010. On the processes linking climate to ecosystem changes. Journal of Marine Systems 79, 374–388.
Dyck, A., Sumaila, U.R., 2010. Economic impact of ocean fish populations in the global fishery. Journal of Bioeconomics 12, 227–243.
Ek, M.B., Mitchell, K.E., Lin, Y., Rogers, E., Grunmann, P., Koren, V., Gayno, G., Tarpley, J.D., 2003. Implementation of Noah land surface model advances in the National Centers for Environmental Prediction operational mesoscale Eta model. Journal of Geophysical Research – Atmospheres 108.
Fisher, R.A., 1915. Frequency distribution of the values of the correlation coefficient in samples from an indefinitely large population. Biometrika 10, 507–521.
Fisher, R.A., 1924. The distribution of the partial correlation coefficient. Metron 3, 329–332.

Frankignoul, C., 1985. Sea-surface temperature anomalies, planetary-waves, and air-sea feedback in the middle latitudes. Reviews of Geophysics 23, 357–390.

Fratantoni, P.S., Pickart, R.S., 2007. The western North Atlantic shelfbreak current system in summer. Journal of Physical Oceanography 37, 2509–2533.

GCOS, 2010. Implementation Plan for the Global Observing System for Climate in Support of UNFCCC (2010 Update). p. 186.

Goddard, L., Mason, S.J., Zebiak, S.E., Ropelewski, C.F., Basher, R., Cane, M.A., 2001. Current approaches to seasonal-to-interannual climate predictions. International Journal of Climatology 21, 1111–1152.

Greene, C.H., Pershing, A.J., 2003. The flip-side of the North Atlantic Oscillation and modal shifts in slope-water circulation patterns. Limnology and Oceanography 48, 319–322.

Griffies, S.M., Harrison, M.J., Pacanowski, R.C., Rosati, A., 2004. A Technical Guide to MOM4. Ocean Group Tech. Rep. 5. Geophysical Fluid Dynamics Laboratory, Princeton, NJ.

Griffies, S.M., Gnanadesikan, A., Dixon, K.W., Dunne, J.P., Gerdes, R., Harrison, M.J., Rosati, A., Russell, J.L., Samuels, B.L., Spelman, M.J., Winton, M., Zhang, R., 2005. Formulation of an ocean model for global climate simulations. Ocean Science 1, 45–79.

Guemas, V., Blanchard-Wrigglesworth, E., Chevallier, M., Day, J.J., Deque, M., Doblas-Reyes, F.J., Fuckar, N.S., Germe, A., Hawkins, E., Keeley, S., Koenigk, T., Salas y Melia, D., Tietsche, S., 2014. A review on Arctic sea-ice predictability and prediction on seasonal to decadal time-scales. Quarterly Journal of the Royal Meteorological Society.

Haltuch, M.A., Punt, A.E., Dorn, M.W., 2009. Evaluating the estimation of fishery management reference points in a variable environment. Fisheries Research 100, 42–56.

Hanawa, K., Sugimoto, S., 2004. 'Reemergence' areas of winter sea surface temperature anomalies in the world's oceans. Geophysical Research Letters 31.

Hawkins, E., Robson, J., Sutton, R., Smith, D., Keenlyside, N., 2011. Evaluating the potential for statistical decadal predictions of sea surface temperatures with a perfect model approach. Climate Dynamics 37, 2495–2509.

Hobday, A.J., Hartog, J.R., 2014. Derived ocean features for dynamic ocean management. Oceanography 27, 134–145.

Hobday, A.J., Hartog, J.R., Spillman, C.M., Alves, O., 2011. Seasonal forecasting of tuna habitat for dynamic spatial management. Canadian Journal of Fisheries and Aquatic Sciences 68, 898–911.

Hobday, A., Maxwell, S., Forgie, J., McDonald, J., Darby, M., Seto, K., Bailey, H., Bograd, S., Briscoe, D., Costa, D., Crowder, L., Dunn, D., Fossette, S., Halpin, P., Hazen, E., Lascelles, B., Lewison, R., Poulos, G., Powers, A., 2014. Dynamic ocean management: integrating scientific and technological capacity with law, policy and management. Stanford Environmental Law Journal 33, 125–168.

Hughes, S.L., Holliday, N.P., Colbourne, E., Ozhigin, V., Valdimarsson, H., Osterhus, S., Wiltshire, K., 2009. Comparison of in situ time-series of temperature with gridded sea surface temperature datasets in the North Atlantic. Ices Journal of Marine Science 66, 1467–1479.

Hunt, G.L., Coyle, K.O., Eisner, L.B., Farley, E.V., Heintz, R.A., Mueter, F., Napp, J.M., Overland, J.E., Ressler, P.H., Salo, S., Stabeno, P.J., 2011. Climate impacts on eastern Bering Sea foodwebs: a synthesis of new data and an assessment of the Oscillating Control Hypothesis. Ices Journal of Marine Science 68, 1230–1243.

IOOS, 2013. U.S. Integrated Ocean Observing System 2013 Report to Congress. p. 55.

Jia, L., Yang, X., Vecchi, G.A., Gudgel, R., Delworth, T., Rosati, A., Stern, W.F., Wittenberg, A., Krishnamurthy, L., Zhang, S., Msadek, R., Kapnick, S., Underwood, S.D., Zeng, F., Anderson, W.G., Balaji, V., Dixon, K., 2015. Improved seasonal prediction of temperature and precipitation over land in a high-resolution GFDL climate model. Journal of Climate 28, 2044–2062.

Jin, E.K., Kinter, J.L., Wang, B., Park, C.K., Kang, I.S., Kirtman, B.P., Kug, J.S., Kumar, A., Luo, J.J., Schemm, J., Shukla, J., Yamagata, T., 2008. Current status of ENSO prediction skill in coupled ocean-atmosphere models. Climate Dynamics 31, 647–664.

Keyl, F., Wolff, M., 2008. Environmental variability and fisheries: what can models do? Reviews in Fish Biology and Fisheries 18, 273–299.

Kirtman, B.P., Min, D., Infanti, J.M., Kinter, J.L., Paolino, D.A., Zhang, Q., van den Dool, H., Saha, S., Mendez, M.P., Becker, E., Peng, P.T., Tripp, P., Huang, J., DeWitt, D.G., Tippett, M.K., Barnston, A.G., Li, S.H., Rosati, A., Schubert, S.D., Rienecker, M., Suarez, M., Li, Z.E., Marshak, J., Lim, Y.K., Tribbia, J., Pegion, K., Merryfield, W.J., Denis, B., Wood, E.F., 2014. The North American multimodel ensemble phase-1 seasonal-to-interannual prediction; phase-2 toward developing intraseasonal prediction. Bulletin of the American Meteorological Society 95, 585–601.

Kristiansen, T., Drinkwater, K.F., Lough, R.G., Sundby, S., 2011. Recruitment variability in North Atlantic cod and match-mismatch dynamics. Plos One 6.

Kwon, Y.O., Alexander, M.A., Bond, N.A., Frankignoul, C., Nakamura, H., Qiu, B., Thompson, L., 2010. Role of the Gulf stream and Kuroshio-Oyashio systems in large-scale atmosphere-ocean interaction: a review. Journal of Climate 23, 3249–3281.

Lagerloef, G., Colomb, F.R., Le Vine, D., Wentz, F., Yueh, S., Ruf, C., Lilly, J., Gunn, J., Chao, Y., deCharon, A., Feldman, G., Swift, C., 2008. The aquarius/Sac-D mission: designed to meet the salinity remote-sensing challenge. Oceanography 21, 68–81.

Large, W.G., Danabasoglu, G., 2006. Attribution and impacts of upper-ocean biases in CCSM3. Journal of Climate 19, 2325–2346.

Lehodey, P., Alheit, J., Barange, M., Baumgartner, T., Beaugrand, G., Drinkwater, K., Fromentin, J.-M., Hare, S., Ottersen, G., Perry, R., Roy, C., van der Lingen, C.D., Werner, F.E., 2006. Climate variability, fish, and fisheries. Journal of Climate 15 (October), 5009–5030.

Livezey, R.E., Smith, T.M., 1999. Covariability of aspects of north American climate with global sea surface temperatures on interannual to interdecadal timescales. Journal of Climate 12, 289–302.

Livezey, R.E., Timofeyeva, M.M., 2008. The first decade of long-lead US seasonal forecasts – insights from a skill analysis. Bulletin of the American Meteorological Society 89, 843–854.

Loder, J., Petrie, B., Gawarkiewicz, G. (Eds.), (1998). The Coastal Ocean off Northeastern North America. A Large-scale View.

Mackas, D.L., Batten, S., Trudel, M., 2007. Effects on zooplankton of a warmer ocean: recent evidence from the Northeast Pacific. Progress in Oceanography 75, 223–252.

Mantua, N.J., Hare, S.R., Zhang, Y., Wallace, J.M., Francis, R.C., 1997. A Pacific interdecadal climate oscillation with impacts on salmon production. Bulletin of the American Meteorological Society 78, 1069–1080.

Maunder, M.N., Watters, G.M., 2001. Status of the yellowfin tuna in the eastern Pacific Ocean. Inter-American Tropical Tuna Commission Stock Assessment Report 1, 5–86.

May, D.A., Parmeter, M.M., Olszewski, D.S., McKenzie, B.D., 1998. Operational processing of satellite sea surface temperature retrievals at the Naval Oceanographic Office. Bulletin of the American Meteorological Society 79, 397–407.

McClatchie, S., Duffy-Anderson, J., Field, J.C., Goericke, R., Griffith, D., Hanisko, D.S., Hare, J.A., Lyczkowski-Shultz, J., Peterson, W.T., Watson, W., Weber, E.D., Zapfe, G., 2014. Long time series in US fisheries oceanography. Oceanography 27, 48–67.

Methot, R.D., 2009. Stock assessment: operational models in support of fisheries management. In: Beamish, R.J., Rothschild, B.J. (Eds.), The Future of Fisheries Science in North America. Springer, New York.

Msadek, R., Vecchi, G.A., Winton, M., Gudgel, R.G., 2014. Importance of initial conditions in seasonal predictions of Arctic sea ice extent. Geophysical Research Letters 41, 5208–5215.

Mueter, F.J., Broms, C., Drinkwater, K.F., Friedland, K.D., Hare, J.A., Hunt, G.L., Melle, W., Taylor, M., 2009. Ecosystem responses to recent oceanographic variability in high-latitude Northern Hemisphere ecosystems. Progress in Oceanography 81, 93–110.

Myers, R.A., 1998. When do environment-recruitment correlations work? Reviews in Fish Biology and Fisheries 8, 285–305.

Namais, J., Born, R.M., 1970. Temporal coherence in North Pacific sea surface temperature patterns. Journal of Geophysical Research 75, 5952–5955.

Namais, J., Born, R.M., 1974. Further studies of the temporal coherence of North Pacific Sea surface temperature. Journal of Geophysical Research 79, 797–798.

Nellemann, C., Hain, S., Alder, J. (Eds.), 2008. Dead Water – Merging of Climate Change with Pollution, Over-harvest, and Infestations in the World's Fishing Grounds. UNEP, GRID-Arendal, Norway.

Newman, M., 2007. Interannual to decadal predictability of tropical and North Pacific Sea surface temperatures. Journal of Climate 20, 2333–2356.

Nye, J.A., Link, J.S., Hare, J.A., Overhultz, W.J., 2009. Changing spatial distribution of fish stocks in relation to climate and population size on the Northeast United States continental shelf. Marine Ecology Progress Series 393, 111–139.

Nye, J.A., Joyce, T.M., Kwon, Y.O., Link, J.S., 2011. Silver hake tracks changes in Northwest Atlantic circulation. Nature Communications 2.

Ottersen, G., Kim, S., Huse, G., Polovina, J.J., Stenseth, N.C., 2010. Major pathways by which climate may force marine fish populations. Journal of Marine Systems 79, 343–360.

Pena, M.A., Bograd, S.J., 2007. Time series of the northeast Pacific. Progress in Oceanography 75, 115–119.

Peng, P.T., Kumar, A., Halpert, M.S., Barnston, A.G., 2012. An analysis of CPC's operational 0.5-month lead seasonal outlooks. Weather and Forecasting 27, 898–917.

Pershing, A.J., Greene, C.H., Hannah, C.G., Mountain, D.G., Sameoto, D., Head, E., Jossi, J.W., Benfield, M.C., Reid, P.C., Durbin, T.G., 2001. Gulf of Maine/Western Scotian Shelf ecosystems respond to changes in ocean circulation associated with the North Atlantic Oscillation. Oceanography 14, 76–82.

Peterson, W.T., Keister, J.E., Feinberg, L.R., 2002. The effects of the 1997–99 El Nino/La Nina events on hydrography and zooplankton off the central Oregon coast. Progress in Oceanography 54, 381–398.

Pinsky, M.L., Mantua, N.J., 2014. Emerging adaptation approaches for climate-ready fisheries management. Oceanography 27, 146–159.

Pinsky, M.L., Worm, B., Fogarty, M.J., Sarmiento, J.L., Levin, S.A., 2013. Marine taxa track local climate velocities. Science 341, 1239–1242.

Planque, B., Fredou, T., 1999. Temperature and the recruitment of Atlantic cod (Gadus morhua). Canadian Journal of Fisheries and Aquatic Sciences 56, 2069–2077.

Punt, A.E., Amar, T., Bond, N.A., Butterworth, D.S., de Moor, C.L., Oliveira, J.A.A., Haltuch, M.A., Hollowed, A.B., Szuwalski, C., 2014. Fisheries management under climate and environmental uncertainty: control rules and performance simulation. Ices Journal of Marine Science 71, 2208–2220.

Quan, X., Hoerling, M., Whitaker, J., Bates, G., Xu, T., 2006. Diagnosing sources of US seasonal forecast skill. Journal of Climate 19, 3279–3293.

Quinn, T.J., Deriso, R.B., 1999. Quantitative Fish Dynamics. Oxford University Press, New York.

Reichler, T., Kim, J., 2008. How well do coupled models simulate today's climate? Bulletin of the American Meteorological Society, 303–311. http://dx.doi.org/10.1175/BAMS-89-3-303.

Reynolds, R.W., Smith, T.M., Liu, C., Chelton, D.B., Casey, K.S., Schlax, M.G., 2007. Daily high-resolution-blended analyses for sea surface temperature. Journal of Climate 20, 5473–5496.

Roads, J.O., 1986. Forecasts of time averages with a numerical weather prediction model. Journal of the Atmospheric Sciences 43, 871–892.

Ropelewski, C.F., Halpert, M.S., 1986. North-American precipitation and temperature patterns associated with the Elnino Southern Oscillation (Enso). Monthly Weather Review 114, 2352–2362.

Ropelewski, C.F., Halpert, M.S., 1987. Global and regional scale precipitation patterns associated with the El-Nino Southern Oscillation. Monthly Weather Review 115, 1606–1626.

Saha, S., Moorthi, S., Pan, H.L., Wu, X.R., Wang, J.D., Nadiga, S., Tripp, P., Kistler, R., Woollen, J., Behringer, D., Liu, H.X., Stokes, D., Grumbine, R., Gayno, G., Wang, J., Hou, Y.T., Chuang, H.Y., Juang, H.M.H., Sela, J., Iredell, M., Treadon, R., Kleist, D., Van Delst, P., Keyser, D., Derber, J., Ek, M., Meng, J., Wei, H.L., Yang, R.Q., Lord, S., Van den Dool, H., Kumar, A., Wang, W.Q., Long, C., Chelliah, M., Xue, Y., Huang, B.Y., Schemm, J.K., Ebisuzaki, W., Lin, R., Xie, P.P., Chen, M.Y., Zhou, S.T., Higgins, W., Zou, C.Z., Liu, Q.H., Chen, Y., Han, Y., Cucurull, L., Reynolds, R.W., Rutledge, G., Goldberg, M., 2010. The NCEP climate forecast system reanalysis. Bulletin of the American Meteorological Society 91, 1015–1057.

Saha, S., Moorthi, S., Wu, X.R., Wang, J., Nadiga, S., Tripp, P., Behringer, D., Hou, Y.T., Chuang, H.Y., Iredell, M., Ek, M., Meng, J., Yang, R.Q., Mendez, M.P., Van Den Dool, H., Zhang, Q., Wang, W.Q., Chen, M.Y., Becker, E., 2014. The NCEP climate forecast system version 2. Journal of Climate 27, 2185–2208.

Schopf, P.S., Suarez, M.J., 1988. Vacillations in a coupled ocean atmosphere model. Journal of the Atmospheric Sciences 45, 549–566.

Sherman, K., Alexander, L.M. (Eds.), 1986. Variability and Management of Large Marine Ecosystems. Westview Press, Boulder.

Smit, A.J., Roberts, M., Anderson, R.J., Dufois, F., Dudley, S.F.J., Bornman, T.G., Olbers, J., Bolton, J.J., 2013. A coastal seawater temperature dataset for biogeographical studies: large biases between in situ and remotely-sensed data sets around the coast of South Africa. Plos One 8.

Spillman, C.M., Alves, O., 2009. Dynamical seasonal prediction of summer sea surface temperatures in the Great Barrier Reef. Coral Reefs 28, 197–206.

Spillman, C.M., Hobday, A.J., 2014. Dynamical seasonal ocean forecasts to aid salmon farm management in a climate hotspot. Climate Risk Management 1, 25–38.

Spillman, C.M., Alves, O., Hudson, D.A., 2011. Seasonal prediction of thermal stress accumulation for coral bleaching in the tropical oceans. Monthly Weather Review 139, 317–331.

Spillman, C.M., Alves, O., Hudson, D.A., 2013. Predicting thermal stress for coral bleaching in the Great Barrier Reef using a coupled oceanatmosphere seasonal forecast model. International Journal of Climatology 33, 1001–1014.

Stabeno, P.J., Bond, N.A., Kachel, N.B., Salo, S.A., Schumacher, J.D., 2001. On the temporal variability of the physical environment over the south-eastern Bering Sea. Fisheries Oceanography 10, 81–98.

Stock, C.A., Alexander, M.A., Bond, N.A., Brander, K.M., Cheung, W.W.L., Curchitser, E.N., Delworth, T.L., Dunne, J.P., Griffies, S.M., Haltuch, M.A., Hare, J.A., Hollowed, A.B., Lehodey, P., Levin, S.A., Link, J.S., Rose, K.A., Rykaczewski, R.R., Sarmiento, J.L., Stouffer, R.J., Schwing, F.B., Vecchi, G.A., Werner, F.E., 2011. On the use of IPCC-class models to assess the impact of climate on Living Marine Resources. Progress in Oceanography 88, 1–27.

Stockdale, T.N., Anderson, D.L.T., Balmaseda, M.A., Doblas-Reyes, F., Ferranti, L., Mogensen, K., Palmer, T.N., Molteni, F., Vitart, F., 2011. ECMWF seasonal forecast system 3 and its prediction of sea surface temperature. Climate Dynamics 37, 455–471.

Sugimoto, S., Hanawa, K., 2007. Impact of remote reemergence of the subtropical mode water on winter SST variation in the central North Pacific. Journal of Climate 20, 173–186.

Szuwalski, C.S., Punt, A.E., 2013. Fisheries management for regime-based ecosystems: a management strategy evaluation for the snow crab fishery in the eastern Bering Sea. Ices Journal of Marine Science 70, 955–967.

Szuwalski, C.S., Vert-pre, K.A., Punt, A.E., Branch, T.E., Hilborn, R., 2013. Examining common assumptions about recruitment: a meta-analysis of recruitment dynamics for worldwide marine fisheries. Fish and Fisheries.

Vecchi, G.A., Delworth, T., Gudgel, R., Kapnick, S., Rosati, A., Wittenberg, A.T., Zeng, F., Anderson, W., Balaji, V., Dixon, K., Jia, L., Kim, H.S., Krishnamurthy, L., Msadek, R., Stern, W.F., Underwood, S.D., Villarini, G., Yang, X., Zhang, S., 2014. On the seasonal forecasting of regional tropical cyclone activity. Journal of Climate 27, 7994–8016.

Vert-pre, K.A., Amoroso, R.O., Jensen, O.P., Hilborn, R., 2013. Frequency and intensity of productivity regime shifts in marine fish stocks. Proceedings of the National Academy of Sciences of the United States of America 110, 1779–1784.

von Storch, H., Zweirs, F.W., 1999. Statistical Analysis in Climate Research. Cambridge University Press.

Walters, C.J., 1989. Value of short-term forecasts of recruitment variation for harvest management. Canadian Journal of Fisheries and Aquatic Sciences 46, 1969–1976.

Walters, C., Martell, S., 2004. Fisheries Ecology and Management. Princeton University Press, Princeton, NJ.

Wang, W.Q., Chen, M.Y., Kumar, A., 2013. Seasonal prediction of Arctic sea ice extent from a coupled dynamical forecast system. Monthly Weather Review 141, 1375–1394.

Weingartner, T.J., Danielson, S.L., Royer, T.C., 2005. Freshwater variability and predictability in the Alaska Coastal Current. Deep-Sea Research Part II – Topical Studies in Oceanography 52, 169–191.

Wen, C.H., Xue, Y., Kumar, A., 2012. Seasonal prediction of North Pacific SSTs and PDO in the NCEP CFS hindcasts. Journal of Climate 25, 5689–5710.

Worley, S.J., Woodruff, S.D., Reynolds, R.W., Lubker, S.J., Lott, N., 2005. ICOADS release 2.1 data and products. International Journal of Climatology 25, 823–842.

Wyrtki, K., 1975. El Nino – the dynamical response of the equatorial Pacific to atmospheric forcing. Journal of Physical Oceanography 5, 572–584.

Xue, Y., Huang, B.Y., Hu, Z.Z., Kumar, A., Wen, C.H., Behringer, D., Nadiga, S., 2011. An assessment of oceanic variability in the NCEP climate forecast system reanalysis. Climate Dynamics 37, 2511–2539.

Zebiak, S.E., Cane, M.A., 1987. A model El-Nino Southern Oscillation. Monthly Weather Review 115, 2262–2278.

Zhang, S., Harrison, M.J., Rosati, A., Wittenberg, A., 2007. System design and evaluation of coupled ensemble data assimilation for global oceanic climate studies. Monthly Weather Review 135, 3541–3564.